# Stereoselective Polymerization of *rac*-Lactide Catalyzed by Zinc Complexes with Tetradentate Aminophenolate Ligands in Different Coordination Patterns: Kinetics and Mechanism

Yang Yang, Haobing Wang, and Haiyan Ma*

Shanghai Key Laboratory of Functional Materials Chemistry and Laboratory of Organometallic Chemistry, East China University of Science and Technology, 130 Meilong Road, Shanghai 200237, P. R. China

Ⓢ *Supporting Information*

ABSTRACT: A series of monomeric zinc silylamido complexes bearing [NNNO]-type tetradentate aminophenolate ligands, $LZnN(SiMe_3)_2$ [L = {(2-R^1)$ArCH_2N[(CH_2)_2R^2$]-$CH_2(4-R^4-6-R^3)C_6H_2O-$}, R^1 = NMe_2, R^2 = N^iPr_2, R^3 = R^4 = Cl (**1**), R^3 = R^4 = cumyl (**3**); R^1 = NMe_2, R^2 = NEt_2, R^3 = R^4 = cumyl (**2**), R^3 = CPh_3, R^4 = Me (**4**); R^1 = NEt_2, R^2 = NEt_2, R^3 = CPh_3, R^4 = Me (**5**); R^1 = NMe_2, R^2 = (S)-1-butylpyrrolidin-2-yl, R^3 = R^4 = cumyl (**6**), R^3 = CPh_3, R^4 = Me (**7**)], have been synthesized via reactions of $Zn[N(SiMe_3)_2]_2$ and 1 equiv of the corresponding aminophenols. The monomeric nature and

versatile coordination patterns of these complexes in the solid state were further confirmed by X-ray diffraction studies on complexes **2**, **3**, **5**, and **7**. In complex **3**, the *N,N*-diisopropylamino group on the pendant side arm does not coordinate to the metal center; only the remaining three donors of the aminophenolate ligand and the silylamido group interact with the zinc center. By contrast, in complexes **2**, **5**, and **7**, the amino group of the aryl moiety does not coordinate to the metal center, while the amino group on the pendant side arm coordinates. At room temperature, the above-mentioned structural features of these complexes are retained in solution, as confirmed by ${}^1H$ NMR spectroscopy. Complexes **1−7** proved to be efficient initiators for the ring-opening polymerization of *rac*-lactide (*rac*-LA) at ambient temperature, and the polymerizations were better controlled in the presence of 2-propanol. The coordination pattern of the aminophenolate ligand exerted a significant influence on the stereoselectivity of the corresponding complex toward the polymerization of *rac*-LA, leading to the production of heterotactic biased polylactides (PLAs) by complexes **1** and **3** (P_m = 0.40−0.46) and moderately to highly isotactic PLAs by complexes **2** and **4−7** (P_m = 0.70−0.81). Detailed kinetic investigations revealed a first-order dependence on the monomer concentration for all complexes and different orders in the initiator concentration ranging from 1.78 to 1.81. The nature of the solvent as well as the molar ratio of the zinc complex and 2-propanol also displayed certain influence on the order of *rac*-LA polymerization in the initiator concentration. Factional orders of 1.80, 1.38, and 1.11 were obtained by using complex **5**/${}^iPrOH$ (1:1) in toluene and tetrahydrofuran and complex **5**/${}^iPrOH$ (1:2) in toluene, respectively. On the basis of DOSY and ${}^1H$ and ${}^{13}C$ NMR studies of zinc alkoxide model complexes "$LZn(OCMe_2COOMe)$" as well as the fractional orders of 1.78−1.81 in the initiator concentration, activation/insertion processes likely involving more than one monomeric active species were then hypothesized.
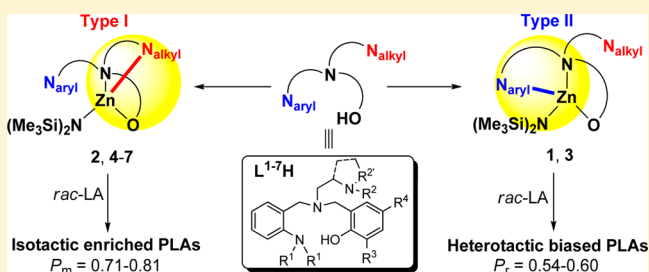
INTRODUCTION

Polylactide (PLA) as a commodity polymer has attracted great attention because of its significant environmental advantages over conventional petrochemically derived plastics.[1] Because of its promising biodegradability, biocompatibility, and biosourced origin, PLA has been used in packaging, agriculture, medicine, pharmaceutics, and tissue engineering fields.[2] These applications, however, are strongly dependent on the microstructures of PLA. For example, amorphous atactic PLA has a glass transition temperature of 60 °C and is subject to a comparatively fast degradation.[2f] On the other hand, isotactic PLA is a crystalline polymer, normally with a T_m of 170 °C in the case of homochiral poly(L-lactide) (PLLA) or poly(D-lactide) (PDLA) or with a T_m up to 230 °C when forming a stereocomplexed structure (obtained by mixing a 1:1 ratio of PLLA and PDLA in solution or melt).[3] Such elevated T_m values

(170−220 °C) can also be achieved for stereoblock isotactic PLAs obtained from the polymerization of *rac*-lactide (*rac*-LA) with highly isoselective initiators.[2b] Because PLA starts to decompose when heated above its melting point, the formation of a stereocomplex becomes an attractive technique to improve its thermal stability.[4] It is therefore rather desired to develop initiators capable of producing isotactic or stereoblock isotactic PLA from *rac*-LA, which is also a much cheaper and accessible starting material than D-LA based on potential industrial applications.

To date, the most straightforward and effective method to prepare isotactic or stereoblock isotactic PLA is the ring-opening polymerization (ROP) of *rac*-LA catalyzed by discrete

metal complexes that could exert a great degree of control over the molecular parameters and chain microstructures of the resultant polymer.[5−9] Examples of isoselective initiators based on metals other than those of group 13 remain extremely rare. Considering the relatively low activity and potential toxicity[10] of aluminum-based catalysts, much effort has been devoted to exploring initiators of other metals, however, unfortunately with poor outcomes. Typically, catalysts based on zinc, alkaline-earth[9a−d] and rare-earth metals[9e−m] often display high heteroselectivity and, only in rare cases, slight isoselectivity toward rac-LA polymerization. Not until very recently have a few rare-earth, zirconium, zinc, and alkali metal complexes been reported to initiate rac-LA polymerization with moderate-to-high isoselectivities, for instance, rare-earth metal complexes supported by phosphine oxide/alkoxide (P_m = ~0.81)[7a] or phosphasalen ligands (P_m = 0.84−0.89),[7b,c] zirconium complexes supported by salan ligands (P_m = 0.65−0.86),[7d] zinc complexes supported by N,N,O-tridentate chiral amino-phenolate (P_m = 0.80−0.84),[8a,e] enantipure scorpinate (P_m = ~0.77),[8b] amidooxazolinate (P_m = ~0.91),[8c] or achiral heteroscorpionate (P_m = ~0.85)[8d] ligands, and sodium and potassium complexes supported by monophenoxides (P_m = 0.63−0.86).[7g]

Our group is interested in using monoanionic amino-phenolate ligands to support the divalent metals, especially some innocuous and colorless metals such as zinc, magnesium, and calcium. The claw-type (scorpionate tripodal geometry) aminophenolate ligands (Chart 1, **I**) proved to provide

Chart 1
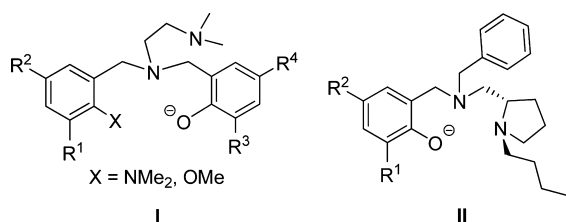
relatively easily adjustable steric hindrance and electronic effect when they wrapped around the divalent metal centers.[11]
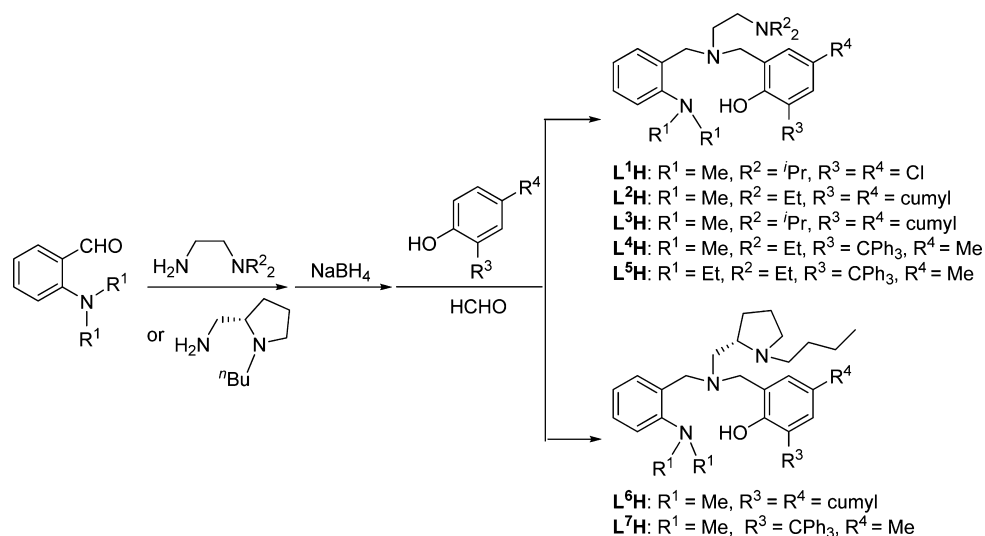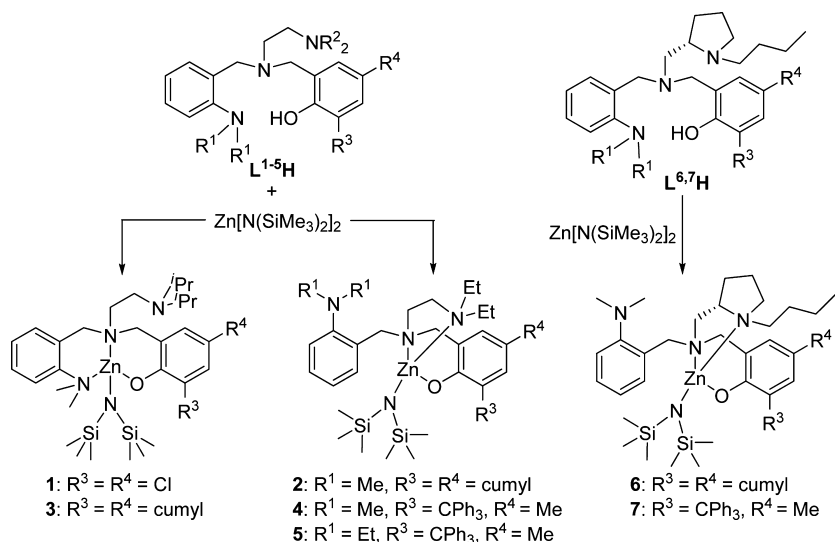
Exceptionally high activities toward the controlled ROP of rac-LA were achieved by using magnesium complexes ligated with methoxy−ether- or dimethylamino-substituted claw-type ami-nophenolate ligands.[11e] The analogous zinc complexes showed slight isoselectivity toward the ROP of rac-LA.[11f] Carpentier's group also reported zinc and magnesium complexes supported by bulky multidentate amino−ether phenolate ligands, which acted as potent precatalysts for the immortal ROP of cyclic esters.[11a] It is recognized that both the ligand structure and the chirality of the initiator play an important role in the stereocontrol during the ROP of rac-LA.[5−9] However, the proper steric hindrance around the metal center,[11a−d] the necessity of containing a chiral group within the ligand framework,[8a,b,e,12] and the coordination efficiency of donor groups of the multidentate ligand are still not clearly identified.[11b] Herein we further modified the claw-type aminophenolate ligands by increasing the steric hindrance of the substituents on alkylamino, arylamino, and phenolate moieties with the expectation of constructing a more stereoselective coordination site for lactide monomers. Besides, the pendant benzyl group in tridentate aminophenolate ligands with a chiral pyrrolidinyl group (Chart 1, **II**), which were reported previously by our group to form zinc complexes of high isoselectivity for rac-LA polymerization,[8a,e] was replaced by an N,N-dimethylanilinyl group, in order to have some insight into the influence of the coordination pattern on the stereoselectivity. Therefore, in this work the preparation and structural characterization of a series of zinc complexes supported by related claw-type tetradentate aminophenolate ligands are reported. Moreover, detailed kinetics for the polymerization of rac-LA initiated by these zinc catalysts along with the effect of solvents and ligand substituents on the rate and stereoselectivity have been investigated.

■ RESULTS AND DISCUSSION

Synthesis and Characterization of Aminophenolate Zinc Complexes. The tetradentate aminophenolate ligands $L^1H−L^7H$ (Scheme 1) with different pendant side arms ($−NCH_2CH_2NEt_2$, $−NCH_2CH_2N^iPr_2$, or $NCH_2[(S)-1-n-bu-tylpyrrolidin-2-yl]$) and arylamine moieties ($−CH_2C_6H_4NMe_2$ or $−CH_2C_6H_4NEt_2$) were constructed as potential ligand

Scheme 1. Synthetic Route of Aminophenol Proligands $L^1H−L^7H$

Scheme 2. Synthetic Route of Complexes 1−7

1: R³ = R⁴ = Cl
3: R³ = R⁴ = cumyl

2: R¹ = Me, R³ = R⁴ = cumyl
4: R¹ = Me, R³ = CPh₃, R⁴ = Me
5: R¹ = Et, R³ = CPh₃, R⁴ = Me

6: R³ = R⁴ = cumyl
7: R³ = CPh₃, R⁴ = Me

platforms of varying sterics to yield stable zinc complexes. According to our previous methods,[8a,11f] the condensation reactions of aryl aldehydes with corresponding alkylamines yielded imine intermediates, which were sequentially reduced to amines without further purification; the crude amines were then treated with substituted phenols and paraformaldehyde via a one-step Mannich condensation reaction to give the target proligands L^1H−L^7H as viscous oils or white microcrystalline powders in moderate-to-high yields. The stoichiometric reactions of L^1H−L^7H with 1 equiv of $Zn[N(SiMe_3)_2]_2$ in toluene at room temperature afforded the corresponding mononuclear zinc silylamido complexes 1−7 (Scheme 2), which were isolated as white powders or microcrystals from chilled n-hexane or toluene/n-hexane solutions in good yields.

All new compounds were characterized by ^1H and ^{13}C NMR spectroscopy as well as elemental analysis. The formation of zinc complexes was confirmed by the disappearance of the hydroxy proton signal and the appearance of one or two new resonances at around 0.01−0.64 ppm assignable to a trimethylsilylamido group bound to the metal center (ZnN-[Si(CH₃)₃]₂). Complexes 1−5 were obtained as racemates. Containing a chiral (S)-pyrrolidinyl group within the ligand framework, complex 6 was obtained as a mixture of two diastereomers in a 10:1 molar ratio, while the ^1H NMR spectrum of complex 7 indicated the existence of a single diastereomer despite the presence of several stereogenic centers. These results are, however, consistent with our previous studies that,[8a,e] when an alkylpyrrolidinyl-derived chiral aminophenolate ligand is adopted to chelate with a zinc center, the introduction of a bulky o-trityl group on the phenoxide ring will enhance the diastereoselectivity during the reaction.

In the ^1H NMR spectrum of complex 1 in C_6D_6, the methyl protons of the $ArN(CH_3)_2$ unit are inequivalent and give rise to two singlets at 2.53 and 2.12 ppm, compared to one sharp peak at 2.37 ppm for the free ligand L^1H. Only one singlet accounting for the two methine protons (2.78 ppm) and two doublets with close chemical shifts (0.93 and 0.91 ppm) assignable to the methyl groups of the diisopropylamino unit are displayed. All of these features suggest that in complex 1 the arylamino group coordinates to the metal center, while the amino group on the alkyl side arm does not. Complex 3

possesses the same coordination pattern in solution as complex 1. Two broad singlets accounting for the $ArN(CH_3)_2$ methyl protons are observed at 2.31 and 1.26 ppm (L^3H, 2.31 ppm). The significant downfield shift of one methyl signal and the broadening of the peaks could be attributed to the shielding effect of the o-cumyl group on the phenolate ring, which has been commonly witnessed in our previous studies when an analogous amino group is coordinated to the metal center and an o-cumyl group is located around it.[11e,f] Moreover, resonances with chemical shifts similar to those of complex 1 are observed for the diisopropylamino group of complex 3. We therefore suggest that in complexes 1 and 3 the tetradentate aminophenolate ligands mainly adopt a tridentate coordination mode upon chelation with the zinc center at ambient temperature, where the more steric bulky alkyl amino group of the ligand is in a dissociated state.

In the case of complex 2, most of the proton resonances of the ligand framework, such as the $ArN(CH_3)_2$ unit, the $N(CH_2CH_3)_2$ unit on the alkyl side arm, methylene groups in the $ArCH_2NCH_2Ar$ unit, and the $−CH_2CH_2$ linkage, however, show fluxional behavior, and broad signals are displayed thoroughly at ambient temperature, as characterized by ^1H NMR spectroscopy. A similar situation could also be observed for complex 4. The fluxionality of complexes 2 and 4 most probably resulted from the hemilabile coordination nature of the ligand. To prove this, variable-temperature (VT) NMR studies of complex 4 in toluene-d_8 were carried out in the temperature range of 208−373 K (Figure S15 in the Supporting Information, SI). At 208 K, two triplets attributable to methyl protons of the $N(CH_2CH_3)_2$ unit can be observed in the uncommonly high-field region (+0.82 and −0.37 ppm), which indubitably indicates coordination of the corresponding alkylamino group to the metal center. As the temperature increases, these two signals become broad and finally coalesce at about 298 K, consistent with the presence of an exchange process between coordinating and noncoordinating states of the alkylamino group. When the temperature further increases, especially above 348 K, only one distinct triplet accounting for the methyl protons of the $N(CH_2CH_3)_2$ unit is observed at 0.68 ppm. During the entire temperature range, the resonance of $ArN(CH_3)_2$ methyl protons shows no significant splitting or broadening, indicative of the noncoordinating state of the

Table 1. Summary of Crystal and Refinement Data for Complexes 2, 3, 5, and 7

	2	3	5	7
empirical formula	$C_{46}H_{70}N_4OSi_2Zn$	$C_{48}H_{74}N_4OSi_2Zn$	$C_{56}H_{80}N_4OSi_2Zn$	$C_{51}H_{70}N_4OSi_2Zn$
fw	816.61	844.66	946.79	876.66
temp (K)	293(2)	293(2)	140(2)	173(2)
cryst size (mm)	0.12 × 0.10 × 0.08	0.313 × 0.157 × 0.102	0.160 × 0.120 × 0.080	0.211 × 0.175 × 0.123
cryst syst	triclinic	monoclinic	triclinic	monoclinic
space group	$P\bar{1}$	$P2(1)/c$	$P\bar{1}$	$P2(1)$
a (Å)	15.942(7)	17.8874(9)	9.2181(17)	12.2864(17)
b (Å)	17.566(8)	14.0473(7)	15.155(3)	14.562(2)
c (Å)	18.151(8)	21.3854(11)	19.882(4)	14.700(2)
α (deg)	107.073(6)	90	93.920	90
β (deg)	92.287(7)	108.9670(10)	102.415	111.497(3)
γ (deg)	102.561(6)	90	98.769	90
volume (Å^3)	4713(3)	5081.8(4)	2666.1(9)	2447.1(6)
Z	4	4	2	2
d_{calc} (mg/m^3)	1.151	1.104	1.179	1.190
abs coeff (mm^{-1})	0.608	0.566	0.546	0.590
$F(000)$	1760	1824	1020	940
θ range (deg)	1.18–25.01	1.77–26.00	1.054–30.531	1.49–26.00
data collected (hkl)	−18 to +16, −20 to +20, −21 to +14	−22 to +18, −17 to +17, −26 to +26	−13 to +13, −21 to +14, −28 to +28	−15 to +15, −17 to +15, −18 to +18
reflns collected/ unique	19676/16304	30062/9991	26603/16012	17381/8560
R(int)	0.0662	0.0649	0.0801	0.0395
max and min transmn	1.000 and 0.531	1.00000 and 0.36228	0.7461 and 0.6354	0.7456 and 0.6663
data/restraints/param	16304/51/1001	9991/16/541	16012/0/589	8560/1/542
GOF on F^2	0.777	1.000	1.017	0.997
final R1, wR2 [$I > 2\sigma(I)$]	0.0556, 0.1089	0.0553, 0.1186	0.0777, 0.1785	0.0401, 0.0921
R1, wR2 (all data)	0.1461, 0.1326	0.1093, 0.1427	0.1714, 0.2394	0.0545, 0.0996
$\Delta\rho_{max}$ and $\Delta\rho_{min}$ (e/Å^3)	0.573 and −0.321	0.405 and −0.258	0.919 and −0.681	0.412 and −0.218

arylamino group. On the basis of these features, it is conceivable that, although bearing slightly bulky substituents, the coordination of the diethylamino group on the pendant alkyl side arm in complex **4** is still more favorable than that on the aryl ring, and the introduction of slightly bulkier ethyl substituents does weaken the coordination ability of this alkylamino group because such a coordination interaction is only stable at 273 K or below. Furthermore, it is worth noting that, with increasing temperature, significant broadening and shifting of ArCH_2N resonances are also observed. Four doublets are displayed at 273 K; among them, two doublets at 4.40 and 3.21 ppm belonging to the same ArCH_2N unit (^2J = 12.0 Hz) broaden and move to each other with increasing temperature, and the chemical shifts of these two resonances at 373 K (3.81 and 3.71 ppm) are quite close to that of the free ligand **L^{4}H** (3.70 ppm). In contrast to their drastic variation, the other two ArCH_2N resonances only broaden and move slightly (4.51−4.37 and 4.09−4.03 ppm) under identical conditions. Therefore, it is considered that, with increasing temperature, dissociation of the pendant alkylamino group enables the free swing/rotation of the noncoordinated arylamino group to some extent, which finally behaves like it does in the free ligand, whereas coordination of the skeleton nitrogen atom (ArCH_2−N-CH_2Ar) to the zinc center is reserved even at high temperature, as is evidenced by the slight variation of two related resonances attributable to NCH_2 adjacent to the phenolate ring.

In contrast to **2** and **4**, with a diethylamino group substituted on the aryl ring, complex **5** exhibits distinct resonances for most

of the protons in its ^{1}H NMR spectrum at room temperature. More interestingly, 10 protons of one NEt$_2$ unit become too broad to be observed. By a comparison with the signals of free ligand **L^{5}H**, the "disappeared" protons could be attributed to the diethylamino group on the alkyl side arm. On the basis of the VT-NMR studies of complex **4**, it is reasonable to suggest that in complex **5** the alkylamino group is coordinated with the metal center in a more stable way than those in complexes **2** and **4**.

Bearing a chiral (S)-pyrrolidinyl group as the side arm, complexes **6** and **7** possess a coordination pattern similar to that of complex **5** in solution; no fluxionality is observed at ambient temperature. Only one singlet is displayed for the methyl protons in the ArN(CH_3)$_2$ unit, and the coupling modes of the methylene protons of the pyrrolidinyl ring and n-butyl group are more complicated than those of the free ligands. Therefore, in solution coordination of the (S)-pyrrolidinyl group instead of the arylamino group to the zinc center could be deduced.

Taking the spectroscopic features of all of these complexes into account, we believe that with the same alkyl substituents the inherent coordination ability of an alkylamino group is stronger than that of an arylamino group; meanwhile, the significant increase of the steric bulkiness of the substitutes on the alkylamino group might make the order inversed. In this work, complexes **1** and **3** with a bulkier diisopropylamino group on the pendant side arm adopt an arylamine-coordinating mode (Scheme 2), which is significantly different from the
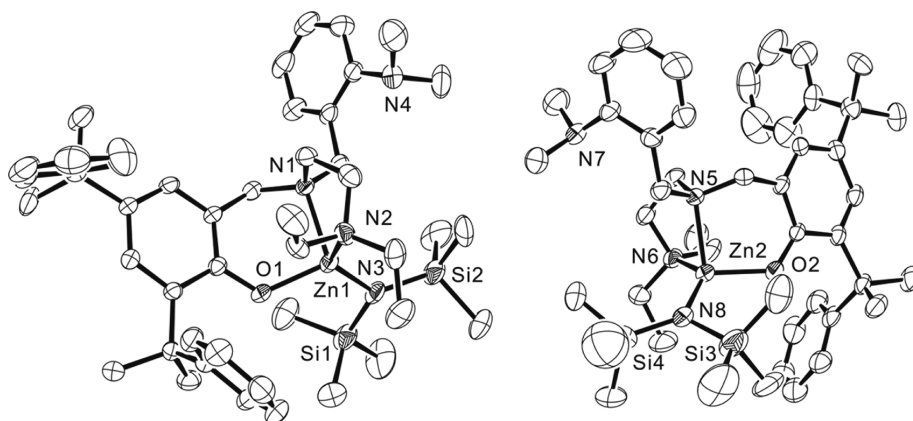
Figure 1. Molecular structure of **2** (ellipsoids drawn at the 30% probability; hydrogen atoms omitted for clarity). Selected bond lengths (Å) and angles (deg): Zn1−N1, 2.130(3); Zn1−N2, 2.166(4); Zn1−N3, 1.949(3); Zn1−O1, 1.935(3); Zn2−N5, 2.144(3); Zn2−N6, 2.164(4); Zn2−N8, 1.908(4); Zn2−O2, 1.951(3); O1−Zn1−N3, 115.98(14); O1−Zn1−N1, 97.09(13); N3−Zn1−N1, 117.34(14); O1−Zn1−N2, 104.29(13); N3−Zn1−N2, 129.52(15); N1−Zn1−N2, 84.53(14); N8−Zn2−O2, 117.00(15); N8−Zn2−N5, 116.85(15); O2−Zn2−N5, 97.12(13); N8−Zn2−N6, 128.55(17); O2−Zn2−N6, 104.63(15); N5−Zn2−N6, 84.42(15).

coordination pattern of complexes **2** and **4**−**7** and those of zinc complexes that we reported previously.[8a,e,11d,f]

Molecular Structures of Complexes 2, 3, 5, and 7. Diffraction-quality crystals of complexes **2**, **3**, **5**, and **7** were obtained from a mixture of toluene/*n*-hexane or benzene/*n*-hexane solution, respectively. Detailed crystal and refinement data are reported in Table 1.

As depicted in Figure 1, two independent molecular structures with identical configurations and slightly different bond angles and lengths were obtained for complex **2**, where both are monomeric and have a tetracoordinated metal center in the solid state. Being consistent with the structure in solution inferred from the ^{1}H NMR spectroscopic study, the alkylamino group does not coordinate to the metal center, as indicated by the considerably long Zn1−N4 distance of 5.180 Å. It must be noted that, upon complexation, the tertiary skeleton nitrogen atom of the ligand framework becomes chiral, and because of chelation of the aminophenolate ligand, the metal center is also chiral. Therefore, although two independent molecules with identical chirality are displayed, in fact the complex exists also as a racemate in the primitive cell.

The coordination environment of complex **3** is different from that of complex **2**, where the arylamino group instead of the alkylamino group coordinates to the zinc center (Figure 2). This difference could be attributed to the large steric hindrance of the diisopropylamine group, preventing its approach to the metal center. The coordination sphere of complex **3** is finally completed by the dimethylamino group on the aryl ring for the reason that a zinc center is inclined to possess a tetracoordinated mode if possible. Besides, the Zn−N$_{aryl}$ bond length [Zn1−N2, 2.168(3) Å] in complex **3** is very close to that of the Zn−N$_{alkyl}$ bond in complex **2** [Zn1−N2, 2.166(4) Å; Zn2−N6, 2.164(4) Å] because of the coordinating nature of the related bonds.

Complex **5** is a structural analogue of complex **2** (Figure 3). It is noted that the distance between the zinc center and the coordinated alkylamino nitrogen atom in complex **5** is somewhat shorter than the corresponding one in complex **2** [Zn1−N2 = 2.149(3) Å in **5**; Zn1−N2 = 2.166(4) Å and Zn2−N6 = 2.164(4) Å in **2**], which may indicate a more hemilabile coordination nature of the Zn−N$_{alkyl}$ bond in complex **2**. Therefore, although the same alkylamino group is involved in
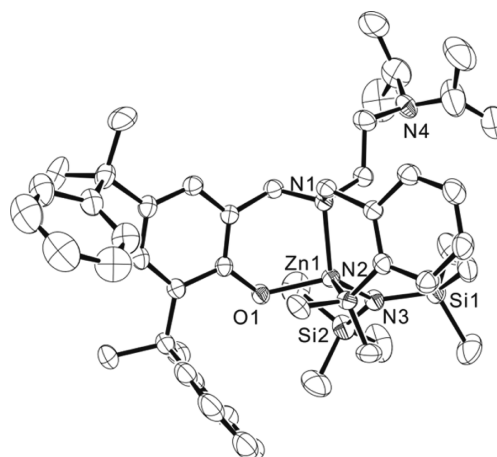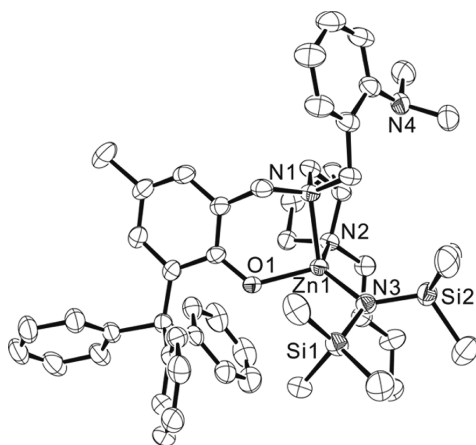

Figure 2. Molecular structure of **3** (ellipsoids drawn at the 30% probability; hydrogen atoms omitted for clarity). Selected bond lengths (Å) and angles (deg): Zn1−N1, 2.097(3); Zn1−N2, 2.168(3); Zn1−N3, 1.925(3); Zn1−O1, 1.943(2); N3−Zn1−O1, 119.57(10); N3−Zn1−N1, 121.01(11); O1−Zn1−N1, 98.46(9); N3−Zn1−N2, 117.80(11); O1−Zn1−N2, 100.71(10); N1−Zn1−N2, 94.38(10).

coordination with the metal center in complexes **2** and **5**, the introduction of a more bulky diethylamino group on the aryl ring in complex **5**, however, stabilizes coordination of the alkylamino group to a certain extent.

As depicted in Figure 4, complex **7** possesses a coordination pattern similar to those of complexes **2** and **5**, where the pendant side arm with a chiral pyrrolidinyl group is coordinated to the zinc center. On the basis of the inherent chirality of the (*S*)-pyrrolidinyl group, an X-ray diffraction study helps to confirm the chirality of each stereogenic center in complex **7**, which can be denoted as $S_C S_N R_N R_{Zn}$ and is identical with that of our previously reported zinc complex **7**′[8a] ligated by a similar tridentate aminophenolate ligand containing the same (*S*)-pyrrolidinyl arm (**7**′: {PhCH$_2$N[CH$_2$-(*S*)-1-butylpyrrolidin-2-yl]-CH$_2$C$_6$H$_2$(*o*-CPh$_3$)(*p*-CH$_3$)O}ZnN(SiMe$_3$)$_2$). The Zn−N and Zn−O bond lengths in complex **7** [Zn1−N3, 1.942(2) Å; Zn1−O1, 1.953(19) Å; Zn1−N2, 2.134(3) Å; Zn1−N1, 2.138(3) Å] are very similar to those of complex **7**′ [Zn1−N3, 1.941(3) Å; Zn1−O1, 1.962(2) Å; Zn1−N2, 2.137(3) Å; Zn1−N1, 2.145(3) Å]. The O1−Zn1−N2 angle of complex **7**
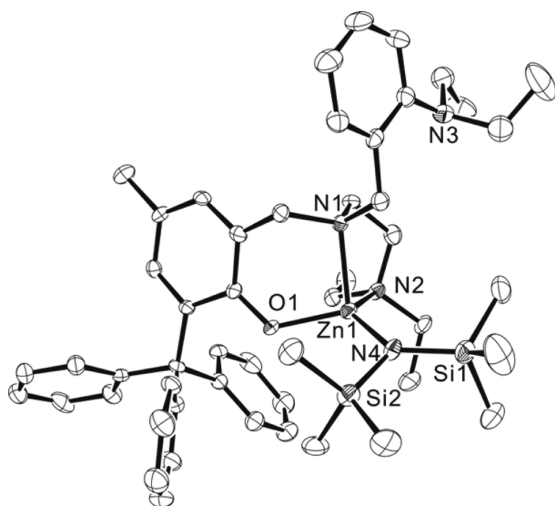
Figure 3. Molecular structure of **5** (ellipsoids drawn at the 30% probability; hydrogen atoms omitted for clarity). Selected bond lengths (Å) and angles (deg): Zn1−N1, 2.140(3); Zn1−N2, 2.149(3); Zn1−N4, 1.937(3); Zn1−O1, 1.947(3); N4−Zn1−O1, 121.00(14); N4−Zn1−N1, 116.38(14); O1−Zn1−N1, 97.48(12); N4−Zn1−N2, 124.78(14); O1−Zn1−N2, 104.16(12); N1−Zn1−N2, 84.42(13).

Figure 4. Molecular structure of **7** (ellipsoids drawn at the 50% probability; hydrogen atoms omitted for clarity). Selected bond lengths (Å) and angles (deg): Zn1−N3, 1.942(2); Zn1−O1, 1.953(19); Zn1−N2, 2.134(3); Zn1−N1, 2.138(3); N3−Zn1−O1, 117.94(9); N3−Zn1−N2, 125.85(11); O1−Zn1−N2, 107.05(10); N3−Zn1−N1, 117.20(14); O1−Zn1−N1, 96.27(10); N2−Zn1−N1, 84.12(11).

[107.05(10)°] is slightly larger than that of complex **7'** [103.70(11)°] because of a more steric 2-(*N,N*-dimethylamino)phenyl group rather than a phenyl ring bonding to the skeleton N1 atom. Moreover, the Zn−N$_{alkyl}$ bond length of complex **7** [Zn1−N2, 2.134(3) Å] is relatively shorter than those of complexes **2** and **5** [2.166(4) and 2.149(3) Å, respectively], indicating a stronger coordination ability of the (*S*)-1-butylpyrrolidin-2-yl group compared to the diethylamino group.

ROP of *rac*-LA. Initially, all of the synthesized zinc silylamido complexes **1−7** were evaluated as single-component initiators for the ROP of *rac*-LA in toluene and tetrahydrofuran (THF) at room temperature (see Table S1 in the SI). Experimental results reveal that all of these complexes display moderate activities for *rac*-LA polymerization and the reactions

can reach completion within a few hours at 25 °C. However, the polymerizations are not well controlled, in most of the cases producing polymers with significantly deviated molecular weights and relatively broad molecular weight distributions (PDI = 1.67−2.51; Table S1 in the SI). According to literature reports, metalsilylamido complexes bearing a variety of ligands such as β-diketiminates,[9a,13] tris(pyrazolyl)borates,[14] and phenoxyimines[15] displayed poor controllability toward the ROP of cyclic esters because of a slow initiation rate relative to that of propagation. It is generally accepted that −N(SiMe$_3$)$_2$ is an inferior initiating group to alkoxy groups such as −O^{i}Pr and −OCH(Me)CO$_2$Me. So, in this work, we mainly focus on the polymerization catalyzed by zinc alkoxides generated in situ.

Before systematic polymerization studies were conducted, the NMR tube reactions of a representative zinc complex with 2-propanol and sequentially with a lactide monomer were conducted first. The typical NMR-scale reaction of complex **4** with 2-propanol in a 1:1 molar ratio clearly indicated the quantitative generation of the target zinc isopropoxide complex "**L^{4}ZnO^{i}Pr**" (Figure S16A in the SI). The 10-fold sequential addition of *rac*-LA to this solution led to a fast oligomerization. No free ligand was detected, and the signals assignable to the isopropyl ester terminus and the methine proton of the last inserted lactate unit of the active propagation chain could be identified unambiguously (Figure S16B in the SI). Although the resonances accounting for the aminophenolate ligand moiety such as the ArCH_2NCH_2Ar unit as well as the −CH_2CH_2 linkage are somewhat complicated, generation of the active oligomer {**L^{4}Zn**[(OCH(CH$_3$)CO)$_n$O^{i}Pr]} is suggested when taking the above-mentioned features into account.

The polymerization of *rac*-LA in toluene and THF employing complexes **1−7** as catalysts in the presence of ^{i}PrOH was then studied in detail. As shown in Table 2, the ROPs of *rac*-LA initiated by the in situ generated zinc isopropoxide complexes are more controlled relative to those by zinc silylamido complexes alone, affording polymers with narrow-to-moderate molecular weight distributions (PDI = 1.08−1.62). Meanwhile, the measured molecular weights (M_n) are still not well-matched to the calculated ones. The catalytic activity is strongly dependent on the structure of the complex and the polymerization conditions. With steric bulky substituents on the alkylamino moiety thus leading to a coordination of the arylamino group to the metal center, complex **3** shows the highest activity in toluene (90% conversion in 20 min; see Table 2, entry 5) among all of these complexes in the presence of 2-propanol. However, complex **1** with a similar coordination pattern but *o*- and *p*-chloro substituents on the phenolate ring requires 90 min to reach 88% monomer conversion under otherwise identical conditions (see Table 2, entry 1), showing the lowest activity among complexes **1−7**. Such an exception may occur on complex **1** for the reason for an electron-withdrawing effect of chloro substituents, which leads to a stronger Zn−OR bonding unfavorable for the insertion of monomer.[10b,16] The introduction of halogens on the ancillary ligand was often reported to have an inconsistent influence on the polymerization. For example, a similar aminophenolate zinc complex, {(2-CH$_3$O)C$_6$H$_4$CH$_2$N[(CH$_2$)$_2$N(CH$_3$)$_2$]CH$_2$(4,6-Cl$_2$)-C$_6$H$_2$O}ZnN(SiMe$_3$)$_2$,[11f] with a methoxy group on the aryl moiety previously reported by our group showed increased catalytic activity when chlorine atoms were substituted at the ortho and para positions of the phenoxy moiety. Being different from complex **1**, this complex adopts an alkylamine-

Table 2. Polymerization of *rac*-LA Catalyzed by Zinc Complexes 1−7 in the Presence of 1 equiv of 2-Propanol[a]

entry	catalyst	solvent	time (min)	conv[b] (%)	$M_{n,calcd}$[c] ($\times 10^4$ Da)	M_n[d] ($\times 10^4$ Da)	PDI[d]	P_m[e]	k_{app} ($\times 10^{-2}$ min^{-1})
1	1	toluene	90	88	2.54	2.33	1.33	0.40	2.47
2	1	THF	120	91	2.61	3.13	1.38	0.41	1.96
3	2	toluene	25	87	2.50	4.27	1.44	0.70	8.66
4	2	THF	55	90	2.58	1.73	1.62	0.70	3.99
5	3	toluene	20	90	2.59	2.44	1.33	0.43	13.1
6	3	THF	50	94	2.70	2.99	1.22	0.46	5.58
7	4	toluene	84	96	2.75	4.53	1.37	0.73	3.25
8	4	THF	150	90	2.59	3.58	1.36	0.72	1.70
9	5	toluene	90	97	2.79	3.69	1.28	0.71	2.52
10	5	THF	240	92	2.66	3.28	1.18	0.70	1.02
11	6	toluene	30	93	2.67	2.74	1.32	0.71	9.42
12	6	THF	60	89	2.55	3.41	1.50	0.72	3.58
13	7	toluene	100	96	2.76	4.26	1.08	0.79	3.54
14	7	THF	120	88	2.52	3.57	1.11	0.81	1.86

[a]Conditions: 25 °C, [*rac*-LA]$_0$ = 1.0 M, [Zn]$_0$ = [^{i}PrOH]$_0$ = 0.005 M. [b]Determined by ^{1}H NMR spectroscopy. [c]$M_{n,calcd}$ = ([LA]$_0$/[^{i}PrOH]$_0$) × 144.13 × conv % + 60. [d]Determined by GPC. [e]P_m is the probability of forming a new *m* dyad, determined by homonuclear-decoupled ^{1}H NMR spectroscopy and calculated by the GSD method.

coordinating mode, which probably accounts for the different influences of chloro substitution on the activity of the corresponding complex. For complexes **2** and **4**−**7** possessing similar coordination environments (with the arylamino group noncoordinated and the alkylamino group coordinated), their activities are mainly affected by the steric hindrance of the ortho substituent on the phenolate ring. Complexes **4**, **5**, and **7**, bearing a trityl group on the ortho position of the phenolate ring, display obviously lower activities than complexes **2** and **6** with a relatively smaller *o*-cumyl group. Such a drastic influence of the steric hindrance of the ortho substituent of the phenolate ring has been commonly observed for other aminophenolate zinc complexes.[8a,11] Besides, the substituents on the dissociated arylamino group also have a certain influence on the catalytic activity. Complex **4** with a smaller dimethylamino group on the aryl moiety shows higher activity than complex **5** with a diethylamino group (Table 2, entries 7−10). It is therefore conceivable that, for complexes **2** and **4**−**7**, the steric hindrances around the metal center involved by the bulky substituents of the phenoxy, arylamino, and alkylamine moieties tend to hinder the approach of a monomer and are disadvantageous to the activity. From the data listed in Table 2, it is also noticed that, out of all with an *o*-cumyl group on the phenolate ring, complex **2** with a coordinated diethylamido group on the side arm shows similar catalytic activity as complex **6** with a pyrrolindinyl one, but both of them are less active than complex **3** with a coordinated dimethylamido group on the aryl ring (Table 2, entries 3, 5, and 11). The similar activities of complexes **2** and **6** might be due to the similar steric bulkiness of two pendant side arms, while a smaller coordinated arylamido group and a different coordination pattern should account for the high activity of complex **3**.

To investigate the exact influence of the ligand substituents on the polymerization rate of *rac*-LA, preliminary kinetic studies were carried out for all complexes in the presence of 2-propanol at 25 °C in toluene and THF, with the concentration of the catalyst fixed at 5 mmol/L and that of monomer at 1.00 mol/L. Table 2 summarizes the apparent propagation rate constants (k_{app}) for these processes, which are consistent with the activity order discussed above. For polymerization runs carried out in toluene, a clear decreasing tendency of the k_{app} values is observed in the order of **3** (Ar-NMe$_2$, alkyl-N^{i}Pr$_2$, and

o-cumyl) > **6** (Ar-NMe$_2$, alkylpyrrolidinyl, and *o*-cumyl) ≥ **2** (Ar-NMe$_2$, alkyl-NEt$_2$, and *o*-cumyl) > **7** (Ar-NMe$_2$, alkylpyrrolidinyl, and *o*-CPh$_3$) ≥ **4** (Ar-NMe$_2$, alkyl-NEt$_2$, and *o*-CPh$_3$) > **5** (Ar-NEt$_2$, alkyl-NEt$_2$, and *o*-CPh$_3$) > **1** (Ar-NMe$_2$, alkyl-N^{i}Pr$_2$, and *o*-Cl).
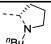
All complexes show higher activity in toluene than in THF. This is in accordance with the results reported by our group[8a,e,11f] and Carpentier's group[11a] using zinc complexes with tridentate or tetradentate aminophenolate ligands or bulky multidentate amino−ether phenolate ligands. The activity decrease in THF is usually attributed to the competed coordination of the solvent with the monomer, while in this work, it might be more complicated because different rate orders in the catalyst concentration have been observed in THF and toluene (vide post).

It is understood that the stereoselectivity of metal complexes toward ROP of *rac*-lactide is closely related with the coordination environment of the active centers in solution. Zirconium alkoxide complexes reported by Kol's group[7e,f] could produce PLAs, with the stereotacticity gradually changing from P_r = 0.73 to P_m = 0.67 via a stepwise adjustment of the substituents and therefore the fluxionality of the ONSO ligand framework. However, they could not determine whether the tacticity was affected primarily by the substitution pattern or by the fluxionality of the catalyst. In this work, under comparable conditions, complexes **1** and **3** show slight heteroselectivity (P_m = 0.40−0.46), while complexes **2** and **4**−**7** afford moderately isotactic PLAs (P_m = 0.71−0.81). In particular, complex **7** exhibits an isoselectivity comparable to that of **7′** (**7′**: P_m = 0.81 at 25 °C; P_m = 0.84 at −38 °C) reported in our previous study,[8a] which to a certain extent implies the ignorable influence of the aryl amino group in **6** and **7** during the polymerization process. Therefore, it is conceivable that the coordination patterns of the aminophenolate ligands in complexes **1**−**7** may play a dominant role in determining their stereoselectivity toward *rac*-LA polymerization, and coordination of the alkyl amino group on the pendant side arm to the metal center is crucial for the moderate isotacticity of complexes **2** and **4**−**7**.

In order to gain better insight into the coordination environment of the propagating species in solution, the reactions of representative complexes **3**, **5**, and **7** and methyl

Table 3. Selected ^{1}H NMR Data of Zinc Complexes 3, 5, and 7 and Zinc Alkoxide Complexes $(L^{3,5,7})Zn(OCMe_2COOMe)$ Generated in Situ^a

Complex	Aryl amino group /ppm		Alkyl amino group /ppm		
	ArN(CH_3)$_2$	ArN(CH_2CH_3)$_2$	N(CH_2CH_3)$_2$	N[CH(CH_3)$_2$]$_2$	(N^{n}Bu)
3	2.31 (s), 1.26 (s)	--	--	0.86 (d), 0.84 (d)	--
$(L^3)Zn(OCMe_2COOMe)$	"disappeared"^{b}	--	--	0.89 (d), 0.90 (d)	--
5	--	0.82 (t)	"disappeared"^{b}	--	--
$(L^5)Zn(OCMe_2COOMe)$	--	0.80 (t)	1.05 (m), −0.03 (m)	--	--
7	2.27 (s)	--	--	--	complicated
$(L^7)Zn(OCMe_2COOMe)$	2.19 (s)	--	--	--	complicated

^{a}In C$_6$D$_6$, 400 MHz, 25 °C. ^{b}Too broad to be assigned properly.

2-hydroxyisobutyrate[17] in C$_6$D$_6$ were monitored by ^{1}H NMR spectroscopy, considering that the in situ generated zinc alkoxide complexes $(L^{3,5,7})Zn(OCMe_2COOMe)$ may serve as model complexes of the propagating species. The selected ^{1}H NMR data are summarized in Table 3.

In comparison with the two broad signals at 2.31 and 1.26 ppm accounting for the aryl-N(CH_3)$_2$ of complex **3**, the corresponding signals of the in situ generated complex $(L^3)Zn(OCMe_2COOMe)$ are too broad to be assigned properly (Figure S17 in the SI). Meanwhile, in the ^{1}H NMR spectrum of $(L^3)Zn(OCMe_2COOMe)$, two doublets assignable to the methyl groups of the diisopropylamino moiety show closed chemical shifts (0.89 and 0.90 ppm) that are also similar to those of complex **3**, therefore implying the noncoordinating state of this alkylamino group in $(L^3)Zn(OCMe_2COOMe)$. Taking all of these features into account, the same coordination pattern of the tetradentate aminophenolate ligand in the silylamido complex **3** is reserved in the formed zinc alkoxide complex $(L^3)Zn(OCMe_2COOMe)$. In the ^{1}H NMR spectrum of $(L^5)Zn(OCMe_2COOMe)$ (Figure S18 in the SI), one triplet at 0.80 ppm and one quartet at 2.66 ppm can be observed, which are quite similar to the corresponding signals of the aryl-N(CH_2CH_3)$_2$ group of complex **5** and should be assigned to the same moiety of $(L^5)Zn(OCMe_2COOMe)$. The hardly changed chemical shifts relative to those of complex **5** also indicate the noncoordinating state of this aryl amino group in $(L^5)Zn(OCMe_2COOMe)$. Coordination of the alkyl amino group to the metal center in $(L^5)Zn(OCMe_2COOMe)$ is evidenced by two separate broad signals, attributed to the methyl groups of the alkyl-N(CH_2CH_3)$_2$ moiety and appearing in uncommonly high fields (1.05 and −0.03 ppm, respectively). Similar spectroscopic features are also observed in the ^{1}H NMR spectrum of the in situ generated zinc alkoxide complex $(L^7)Zn(OCMe_2COOMe)$ (Figure S19 in the SI).

In short, the aminophenolate ligands, in all of these zinc alkoxide complexes generated from zinc silylamido complexes and methyl 2-hydroxyisobutyrate, retain the same coordination pattern because they are in the starting silylamido complexes. Because no significant fluxional behavior has been observed for these zinc alkoxide model complexes at room temperature on the NMR time scale, the possibility proposed by Kol and co-workers that the tacticity of the resultant polymer is mainly affected by the fluxionality of the catalysts is therefore ruled out.[7e,f] As suggested above, the different coordination pattern of the tetradentate aminophenolate ligand in complexes **1−7**, which is controlled by the relative steric bulkiness and

coordination ability of two amino groups, does determine the stereoselectivity of these complexes toward the ROP of *rac*-LA.

Kinetic and Mechanistic Studies. Kinetic studies of *rac*-LA polymerization initiated by complexes **1−7** in the presence of 2-propanol were carried out in toluene and THF at 25 °C ([LA]$_0$/[Zn]$_0$ = 200; [Zn]$_0$ = 5.00 mM; [LA]$_0$ = 1.00 M). In each case, the kinetics of a first-order dependence on the monomer concentration were observed, as evidenced from the linear relationship between ln([LA]$_0$/[LA]$_t$) and time (Figures 5 and S23 in the SI). Thus, the polymerization proceeds
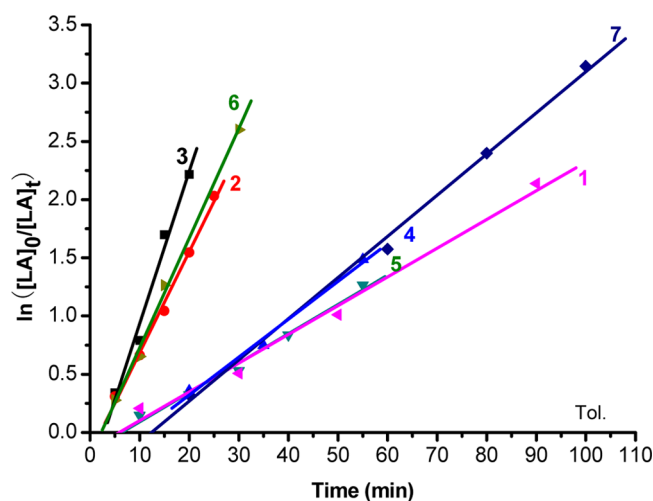

Figure 5. Semilogarithmic plots of ln([LA]$_0$/[LA]$_t$) versus time for *rac*-LA polymerization initiated by complexes **1−7**/^{i}PrOH in toluene at 25 °C [**1** (pink ◀), $y = -0.145 + 0.0247x$, $R = 0.993$; **2** (red ●), $y = -0.181 + 0.0866x$, $R = 0.997$; **3** (■), $y = -0.373 + 0.0131x$, $R = 0.991$; **4** (blue ▲), $y = -0.675 + 0.0325x$, $R = 0.995$; **5** (blue ▼), $y = -0.160 + 0.0252x$, $R = 0.999$; **6** (green ▶), $y = -0.214 + 0.0942x$, $R = 0.998$; and **7** (◆), $y = -0.438 + 0.0354x$, $R = 0.998$; [LA]$_0$ = 1.00 M, [Zn]$_0$ = 5 mmol/L, and [LA]$_0$:[Zn]$_0$:[^{i}PrOH]$_0$ = 200:1:1].

according to the rate law d[LA]/dt = k_{app}[LA], where k_{app} = k_p[Zn]^x, in which k_{app} and k_p are the apparent propagation and propagation rate constant, respectively.

Representative complexes **3**, **5**, and **7** were chosen to study the order of polymerization in the initiator. Various concentrations of catalysts **3**/^{i}PrOH (5.00−1.67 mmol/L), **5**/^{i}PrOH (10.00−2.50 mmol/L), and **7**/^{i}PrOH (10.0−3.33 mmol/L) were used in combination with a fixed monomer concentration of [*rac*-LA] = 1.0 mol/L. All polymerization runs were carried out in toluene at 25 °C. When ln k_{app} versus ln [Zn] was plotted, unexpectedly, nonintegral orders in [Zn] of

1.81 ± 0.04 for $3/^i$PrOH, 1.80 ± 0.08 for $5/^i$PrOH, and 1.78 ± 0.002 for $7/^i$PrOH were obtained (see Figures 6 and S24–S26
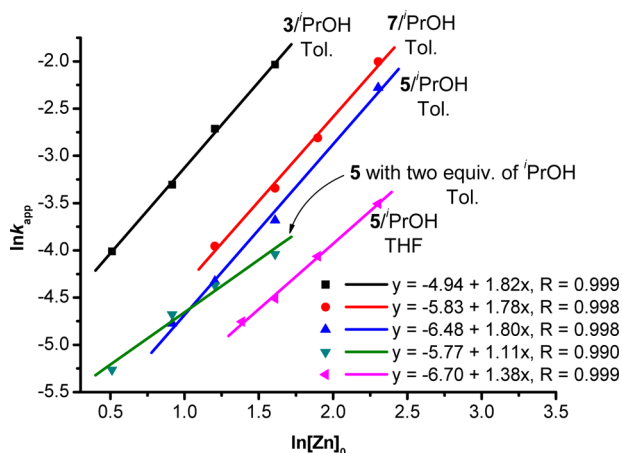
Figure 6. Plot of ln k_{app} versus ln $[Zn]_0$ for polymerization of *rac*-LA (1.00 M) using catalysts **3**, **5**, and **7** at 25 °C.

in the SI). The kinetics of *rac*-LA polymerization using complex $5/^i$PrOH (4.00–10.00 mmol/L) in THF or complex **5** with 2 equiv of 2-propanol in toluene were further studied at 25 °C (Figures S27 and S28 in the SI). As shown in Figure 6, plots of ln k_{app} versus ln $[Zn]$ are still linear but with smaller slopes of 1.38 ± 0.05 and 1.11 ± 0.11, respectively, in comparison with that of $5/^i$PrOH in toluene (1.80 ± 0.08).

A fractional dependency on the initiator concentration has been observed for complexes of sodium,[18] iron,[19] zinc,[9a,20,21] and rare-earth metals.[9e] Normally, an aggregation–dissociation equilibrium between monomeric and multiple nuclear species is suggested to be involved. One example is that the complex is mononuclear both in solution and in the solid state, such as bis(amidinate)iron alkoxide complexes,[19] exhibiting fractional order in the catalyst: $-d[CL]/dt = k_p[CL][L_2FeOCHPh_2]^{0.5}$. This has been interpreted to arise from an aggregation of active polymer chains, with the propagation rate of the aggregated species slower than that of the nonaggregated form. The binuclear (β-diiminate)zinc alkoxide complex,[9a] retaining its binuclear form in solution, also exhibits a fractional order in the catalyst: $-d[LA]/dt = k_p[LA][Zn]^{1.56}$. However, the mechanism study was retarded for the reason that the nature of active

species in their systems appears to be more complicated than anticipated. Another example involves catalysts being binuclear in the solid state but mononuclear in solution. For instance, the (diaminophenolate)zinc alkoxide complex[21] reported by Tolman and co-workers shows a fractional dependency on the catalyst with a rate order of $x = 1.33$ (0 °C) or 1.75 (25 °C). In this case, plots of k_{app} versus $[Zn]$ are linear, and the nonintegral order obtained via semilogarithmic analysis was suggested to be attributed to impurities. Moreover, it has been reported that the dizinc monoalkoxide complex[20] supported by a dinucleating aminophenolate ligand is first-order in the concentration of the dinuclear complex, which is consistent with a bimetallic coordination insertion mechanism. Therefore, the factors causing fractional dependency are somewhat complicated and closely rely on the nature or property of the initiator.

Such nonintegral orders in the catalyst concentration are difficult to interpret mechanistically, although models that incorporate complicated aggregation phenomena or impurities have been postulated for some cases. According to Tolman et al.'s report,[21] if impurities, catalyst deactivators, or chain exchange agents are responsible for the nonintegral order in the catalyst obtained via logarithmic analysis, a threshold catalyst concentration, below which polymerizations will not occur, and lower than predicted polymer molecular weights would be observed as direct support. Actually in Tolman et al.'s work, when k_{app} is plotted versus [catalyst], a linear relationship could still be obtained, which indicates a first-order dependency of the polymerization rate on the catalyst. However, all of these features are not observed in this work. In most cases, the molecular weights of the resultant polymer samples are still higher than the calculated values, and in particular the plots of k_{app} versus $[Zn]$ are not linear (see Table 2 and Figure S29 in the SI), so the effect of impurities as a possible explanation for the fractional dependency in the catalyst should be ruled out.

To understand whether nonintegral orders of around 1.1– 1.8 in the initiator concentration found in this work suggest some aggregation processes of the active species during the polymerization, the nuclearities of the in situ generated zinc alkoxide complexes "LZnO^{i}Pr" and "LZn(OCMe$_2$COOMe)" were determined to have some insight into this hypothesis. According to literature reports, the measurement of the hydrodynamic radius could serve as an effective protocol to probe the nuclearity of the metal species. For example, the

Table 4. DOSY Measurements (298 K) and X-ray Crystallographic Data for (L^4)ZnO^{i}Pr, (L^5)ZnO^{i}Pr, (L^5)Zn(OCMe$_2$COOMe), (L^7)Zn(OCMe$_2$COOMe), 5, and 7^a

				X-ray		
complex	solvent	$D_t{}^b$ (×10^{-10} m^2/s)	$r_H{}^c$	a (Å)	b (Å)	$r_{X\text{-ray}}{}^d$ (Å)
(L^4)ZnO^{i}Pr	benzene-d_6	5.65	6.36			
(L^4)ZnO^{i}Pr	THF-d_8	7.29	6.20			
(L^5)ZnO^{i}Pr	benzene-d_6	5.61	6.40			
(L^5)Zn(OCMe$_2$COOMe)	benzene-d_6	5.24	6.78			
(L^7)Zn(OCMe$_2$COOMe)	benzene-d_6	5.14	7.00			
5				8.26	4.58	6.78
7				7.89	5.46	6.98

^{a}(L^4)ZnO^{i}Pr and (L^5)ZnO^{i}Pr were prepared in situ by mixing complex **4** or **5** with 2-propanol in a molar ratio of 1:1; (L^5)Zn(OCMe$_2$COOMe) and (L^7)Zn(OCMe$_2$COOMe) were prepared in situ by mixing complex **5** or **7** with methyl 2-hydroxyisobutyrate in a molar ratio of 1:1. Concentration of all complexes and TMS: 10.0 mmol/L. $^b D_t$, translational diffusion coefficients, measured by DOSY. $^c r_H$, calculated hydrodynamic radius from D_t. ^{d}Calculated according to $r_{X\text{-ray}} = (a^2b)^{1/3}$, where a and b are respectively the longest and shortest semiaxes of the prolate ellipsoid formed by the complex and are determined from the solid-state structures.

Scheme 3. Structures of Zinc Alkoxide Model Complexes LZn(OCMe$_2$COOMe) (Only One of the Possible Isomers of Each Structure Is Displayed)
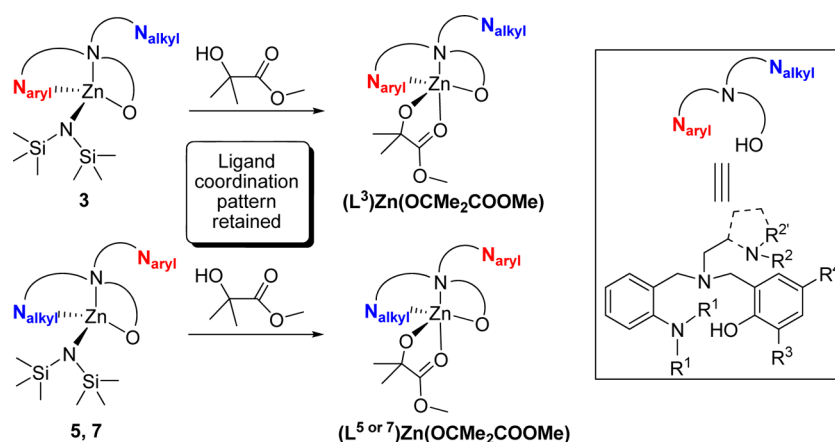

hydrodynamic radius of the zinc alkoxide complex (r_H = 4.9 Å) bearing half of a salan-type phenolate ligand[21] determined by PGSE measurement is ca. 25% smaller than the radius estimated from the X-ray crystal structure of the dinuclear form (r_{X-ray} = 6.8 Å) and is close to that of the corresponding zinc ethyl complex (r_H = 4.2 Å). On the basis of those data, the author concluded that the half salan-type zinc alkoxide complex did not retain its dimeric form in solution. Therefore, the nuclearities of complexes ($L^{4,5}$)ZnO^{i}Pr and ($L^{5,7}$)Zn-(OCMe$_2$COOMe) generated in situ in solution were assessed by diffusion-ordered NMR spectroscopy (DOSY), following protocols developed for zinc and alkaline-earth complexes.[21,22] All measurements were performed at 293 K in C$_6$D$_6$ or THF-d_8, using tetramethylsilane (TMS) as the internal reference.[23] The experimentally determined values of D_t (translational diffusion coefficient) and therefore calculated values of r_H and r_{X-ray} are listed in Table 4 (see the SI for detailed calculation methods). The solution hydrodynamic radius measured in THF-d_8 for (L^4)ZnO^{i}Pr by DOSY (r_H = 6.20 Å) is similar to that determined in benzene-d_6 (r_H = 6.36 Å), evidencing that the zinc isopropoxide complex holds the same structure in these two solvents. A comparison of the hydrodynamic radii of (L^5)ZnO^{i}Pr (r_H = 6.40 Å) and (L^5)Zn(OCMe$_2$COOMe) (r_H = 6.78 Å) determined by DOSY experiments with the X-ray radius of complex **5** estimated from its solid-state structure (r_{X-ray} = 6.78 Å) further suggests that the zinc alkoxide species (L^5)ZnO^{i}Pr and (L^5)Zn(OCMe$_2$COOMe) should both be in a monomeric form in benzene-d_6. Similar results are obtained for (L^7)ZnOR species.

Furthermore, resonances for the C=O moiety in the ^{13}C{^{1}H} NMR spectra of the in situ generated ($L^{3,5,6}$)Zn-(OCMe$_2$COOMe)[24] in C$_6$D$_6$ were detected at δ(C=O) = 185.0–187.6 ppm (Figures S20–S22 in the SI). These downfield shifts with respect to the corresponding resonances of methyl 2-hydroxyisobutyrate (178.2 ppm) demonstrate the coordination of carbonyl to the metal center.[8e,25] It is therefore suggested that zinc alkoxide model complexes LZn-(OCMe$_2$COOMe) regardless of the coordination patterns of the aminophenolate ligands should possess pentacoordinated structures in solution (Scheme 3), similar to the zinc lactate model complexes of the enantiomer of complex **7'**, where pentacoordinated cores are demonstrated in the solid state.[8e]

On the basis of DOSY and ^{13}C NMR studies concerning zinc alkoxide model complexes "LZn(OCMe$_2$COOMe)", it is conceivable that the active species, at least their resting states in the polymerization, are also monomeric and have a pentacoordinated metal core. Because the 1.78–1.81th orders with respect to the catalyst concentration do indicate that two metal centers are likely involved in the rate-determining step of the polymerization, we suggest that in the rate-determining step each lactide monomer is probably activated by one monomeric zinc species but inserts into the Zn–O bond of another monomeric zinc species. In the presence of coordinative molecules (THF, excess isopropyl alcohol), the decrease of the polymerization order in the catalyst concentration might be due to the decreased Lewis acidity of the metal center, which is unfavorable for the above-proposed bimetallic process. Moreover, the nonintegral order (x) in the catalyst concentration under adopted conditions is equal to neither 1 nor 2, which implies that the polymerization might undergo both mono-metallic and bimetallic processes. According to the proposed mechanism, the preferential configuration of the inserted monomer is still chosen by a monomeric active site, which explains well that for a given complex consistent stereo-selectivity toward *rac*-LA polymerization was obtained in different reaction media.

As shown in Figure 7, the linear relationship of a M_n versus monomer conversion plot ([LA]$_0$ = 1.0 M, [LA]$_0$:[^{i}PrOH]$_0$: [7]$_0$ = 200:1:1, at 25 °C in toluene and THF) in conjunction with the narrow polydispersities (PDI < 1.1), indicates that the polymerization proceeded in a living manner. However, molecular weights higher than calculated values (based on [LA]$_0$/[Zn]$_0$) are observed for PLAs obtained both in THF and in toluene. Similar results are also found for complexes **2** and **4–6**,[26] implying that during the polymerization process not all of the zinc species are involved in the propagation of the polymer chain. Because the kinetics of nonintegral orders (1 < x < 2) in the initiator have been followed by these zinc initiators, we think that such deviations of the molecular weights may be a result of the aforeproposed mono- and bimetallic activation/insertion processes. Moreover, as shown in Table 2, the polymers obtained by **1–6**/^{i}PrOH systems show relatively broad polydispersities (1.18–1.62), which might be a further support to the existence of multiple active species in the catalytic system.
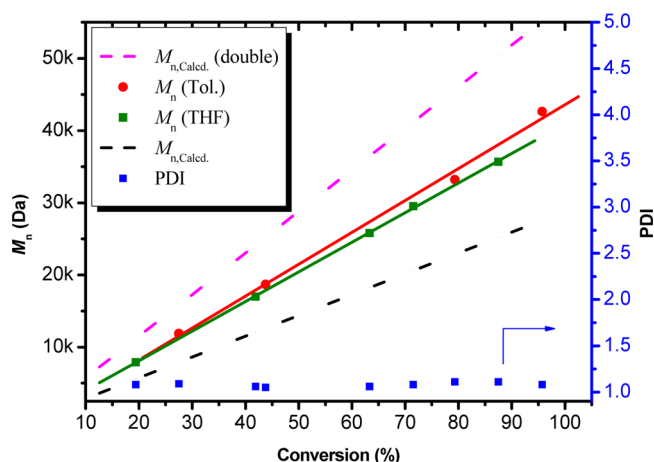
Figure 7. Relationships of M_n and PDI of PLA samples versus monomer conversion obtained from *rac*-LA by complex **7** ($[LA]_0 = 1.0$ M, $[LA]_0 : [^iPrOH]_0 : [7]_0 = 200:1:1$, at 25 °C in toluene (red ●) and THF (gray ■); $M_{n,calcd} = ([LA]_0 / [^iPrOH]_0) \times 144.13 \times$ conv % + 60; $M_{n,calcd}$(double) = $2M_{n,calcd}$, assuming that two zinc centers are involved in the propagation of one polymer chain).

■ CONCLUSIONS

A series of monomeric zinc silylamido complexes **1–7** supported by tetradentate aminophenolate ligands were synthesized and structurally characterized. X-ray diffraction studies revealed that all complexes possess a tetracoordinate zinc center. Being consistent with the solid-state structure of complex **3**, zinc centers in complexes **1** and **3** are coordinated by the aryl amino group instead of the alkyl amino group on the pendant side arm in solution at room temperature, while for complexes **2** and **4–7**, the alkyl amino group instead of the aryl amino group coordinates to the zinc atom. All zinc silylamido complexes **1–7** in the presence of alcohol or not acted as effective initiators for the ROP of *rac*-lactide, with the stereoselectivity closely relying on the coordination pattern of the tetradentate aminophenolate ligand. All complexes with ligands featuring arylamine coordination led to slightly heterotactic PLA, whereas complexes with ligands featuring alkylamine coordination led to isotactic PLA. Detailed kinetic studies of *rac*-LA polymerization initiated by representative zinc silylamido complexes in the presence of ^iPrOH revealed the nonintegral orders in [Zn] from 1.78 to 1.81. Variations of solvents as well as the amount of added alcohol also resulted in a change in the polymerization order in [Zn] ($x = 1.11–1.38$). On the basis of DOSY, ^1H, and ^{13}C NMR studies of zinc alkoxide model complexes "LZn(OCMe$_2$COOMe)" as well as the nonintegral orders of 1.78–1.81 in the initiator concentration discoverd in kinetic studies, a bimetallic process where in the rate-determining step each lactide monomer is probably activated by one monomeric zinc species but inserts into the Zn–O bond of another monomeric zinc species was then hypothesized.

■ EXPERIMENTAL SECTION

Materials and Methods. All manipulations were carried out under a dry argon atmosphere using standard Schlenk-line or glovebox techniques. Toluene and *n*-hexane were refluxed over sodium benzophenone ketyl prior to use. Benzene-d_6, toluene-d_8, chloroform-d, and other reagents were carefully dried and stored in a glovebox. *rac*-Lactide (*rac*-LA; Aldrich) was recrystallized with dry toluene and then sublimed twice under vacuum at 80 °C. 2-Propanol

was dried over calcium hydride under argon prior to distillation. (*S*)-(1-*n*-Butylpyrrolidin-2-yl)methanamine was synthesized according to a previous method reported by our group.[8a] All other chemicals were commercially available and used after appropriate purification. Glassware and vials used in the polymerization were dried in an oven at 120 °C overnight and exposed to a vacuum–argon cycle three times.

Methods. NMR spectra were recorded on Bruker AVANCE-400 and Bruker AVANCE-500 spectrometers at 25 °C (^1H, 400 and 500 MHz; ^{13}C, 100 MHz) unless otherwise stated. Chemical shifts for ^1H and ^{13}C NMR spectra were referenced internally using the residual solvent resonances and reported relative to TMS. Elemental analyses were performed on an EA-1106 instrument. Spectroscopic analyses of polymers were performed in CDCl$_3$. Gel permeation chromatography (GPC) analyses were carried out on a Waters instrument (M1515 pump, Optilab Rex injector) in THF at 35 °C, at a flow rate of 1 mL/min. Calibration standards were commercially available narrowly distributed linear polystyrene samples that cover a broad range of molar masses (10^3 g/mol < M_n < 2×10^6 g/mol).

Syntheses. *4,6-Dichlorido-2-{N-[2-(N′,N′-dimethylamino)-benzyl]-N-[2-(N″,N″-diisopropylamino)ethyl]aminomethyl}phenol* (**L^{1}H**). A mixture of 2-(dimethylamino)benzaldehyde (1.9 g, 12 mmol), *N,N*-diisopropylethane-1,2-diamine (1.8 g, 12 mmol), and sodium sulfate (1.9 g, 12 mmol) in ethanol was heated to reflux for 24 h. After cooling to room temperature, NaBH$_4$ (0.94 g, 25 mmol) was added sequentially to the above yellow solution at 0 °C, and the mixture was stirred at 50 °C for 5 h. All of the volatiles were then evaporated, and the resultant residue was extracted with ethyl acetate (80 mL) and H$_2$O (50 mL). The organic phase was washed with saturated NaHCO$_3$ (2 × 40 mL) and dried with anhydrous MgSO$_4$. After filtration, the filtrate was concentrated to dryness to afford a yellow viscous oil, to which was added a solution of paraformaldehyde (0.45 g, 15 mmol) and 2,4-dichlorophenol (2.4 g, 15 mmol) in ethanol (50 mL). The resultant mixture was heated to 85 °C and stirred for 24 h. After cooling to room temperature, the reaction mixture was concentrated to dryness under vacuum. The resultant yellow residue was purified by column chromatography (PE:EA = 20:1) to give a light-yellow oil characterized as the target product (3.1 g, 45%). ^1H NMR (CDCl$_3$, 400 MHz): δ 7.37 (dd, 1H, ^3J = 7.6 Hz, ^4J = 1.4 Hz, Ar*H*), 7.25–7.21 (m, 2H, Ar*H*), 7.12 (dd, 1H, ^3J = 8.0 Hz, ^4J = 0.8 Hz, Ar*H*), 7.08 (td, 1H, ^3J = 7.6 Hz, ^4J = 0.8 Hz, Ar*H*), 6.88 (d, 1H, ^4J = 2.4 Hz, Ar*H*), 3.76 (s, 4H, ArC*H$_2$*N), 2.85 (hept, 2H, ^3J = 6.4 Hz, N[C*H*(CH$_3$)$_2$]$_2$), 2.64 (s, 6H, ArN(C*H$_3$*)$_2$), 2.54–2.5 (m, 2H, NC*H$_2$*CH$_2$N), 2.46–2.42 (m, 2H, NCH$_2$C*H$_2$*N), 0.87 (d, 12H, ^3J = 6.4 Hz, N[CH(C*H$_3$*)$_2$]$_2$). ^1H NMR (C$_6$D$_6$, 400 MHz): δ 11.4 (br, 1H, O*H*), 7.34 (d, 1H, ^3J = 7.2 Hz, Ar*H*), 7.24 (d, 1H, ^4J = 2.4 Hz, Ar*H*), 7.04 (td, 1H, ^3J = 7.6 Hz, ^4J = 1.2 Hz, Ar*H*), 6.90 (t, 1H, ^3J = 8.0 Hz, Ar*H*), 6.87 (d, 1H, ^3J = 8.0 Hz, Ar*H*), 6.67 (d, ^4J = 2.4 Hz, 1H), 3.51 (s, 2H, ArC*H$_2$*N), 3.29 (s, 2H, ArC*H$_2$*N), 2.72 (hept, ^3J = 6.4 Hz, 2H, N[C*H*(CH$_3$)$_2$]$_2$), 2.37 (s, 6H, ArN(C*H$_3$*)$_2$), 2.37 (m, 2H, NC*H$_2$*CH$_2$N), 2.31 (m, 2H, NCH$_2$C*H$_2$*N), 0.80 (d, 12H, ^3J = 6.4 Hz, N[CH(C*H$_3$*)$_2$]$_2$). ^{13}C NMR (CDCl$_3$, 100 MHz): δ 153.6, 152.8, 131.3, 130.7, 128.6, 128.5, 127.0, 125.2, 123.8, 123.1, 121.5, 119.7 (all Ar*C*), 58.2 (Ar*C*H$_2$N), 54.9 (Ar*C*H$_2$N), 54.0 (N*C*H$_2$CH$_2$N), 49.1 (N[*C*H(CH$_3$)$_2$]$_2$), 45.4 (N(*C*H$_3$)$_2$), 42.8 (NCH$_2$*C*H$_2$N), 20.5 (N[CH(*C*H$_3$)$_2$]$_2$). Anal. Calcd for C$_{24}$H$_{35}$Cl$_2$N$_3$O: C, 63.71; H, 7.80; N, 9.29. Found: C, 63.70; H, 7.79; N, 9.24.

4,6-Dicumyl-2-{N-[2-(N′,N′-dimethylamino)benzyl]-N-[2-(N″,N″-diethylamino)ethyl]aminomethyl}phenol (**L^{2}H**). The procedure was the same as that of **L^{1}H**, except that 2-(dimethylamino)benzaldehyde (1.9 g, 12 mmol), *N,N*-diethylethane-1,2-diamine (1.4 g, 12 mmol), sodium sulfate (1.9 g, 12 mmol), NaBH$_4$ (0.94 g, 25 mmol), paraformaldehyde (0.45 g, 15 mmol), and 2,4-dicumylphenol (4.9 g, 15 mmol) were used to afford **L^{2}H** as a viscous oil (3.6 g, 48%). ^1H NMR (CDCl$_3$, 400 MHz): δ 10.17 (br, 1H, O*H*), 7.26–7.09 (m, 12H, Ar*H*, overlapped with the CDCl$_3$ signal), 7.02 (d, 1H, ^3J = 8.0 Hz, Ar*H*), 6.95 (d, 1H, ^3J = 7.2 Hz, Ar*H*), 6.87 (t, 1H, ^3J = 7.2 Hz, Ar*H*), 6.78 (br s, 1H, Ar*H*), 3.57 (s, 2H, ArC*H$_2$*N), 3.54 (s, 2H, ArC*H$_2$*N), 2.56 (s, 6H, N(C*H$_3$*)$_2$), 2.36–2.29 (m, 4H, NC*H$_2$*CH$_2$N), 2.22 (q, 4H, ^3J = 7.2 Hz, N(C*H$_2$*CH$_3$)$_2$), 1.68 (s, 6H, C(C*H$_3$*)$_2$Ph), 1.67 (s, 6H,

C(CH_3)$_2$Ph), 0.78 (t, 6H, ^3J = 7.2 Hz, N(CH$_2$CH_3)$_2$). ^{1}H NMR (C$_6$D$_6$, 400 MHz): δ 10.48 (s, 1H, OH), 7.57 (d, 1H, ^4J = 2.0 Hz, ArH), 7.45 (d, 2H, ^3J = 7.2 Hz, ArH), 7.36 (d, 2H, ^3J = 7.2 Hz, ArH), 7.21 (t, 2H, ^3J = 7.6 Hz, ArH), 7.18−7.08 (m, 5H, ArH), 6.96 (d, 2H, ^3J = 7.2 Hz, ArH), 6.94 (d, 1H, ^4J = 2.0 Hz, ArH), 6.87 (d, 1H, ^3J = 7.6 Hz, ArH), 3.59 (s, 2H, ArCH_2N), 3.36 (s, 2H, ArCH_2N), 2.33 (s, 6H, ArN(CH_3)$_2$), 2.27−2.24 (m, 2H, NCH$_2$CH_2N), 2.11−2.06 (m, 6H, NCH$_2$CH_2N and N(CH_2CH$_3$)$_2$), 1.87 (s, 6H, C(CH_3)$_2$Ph), 1.73 (s, 6H, C(CH_3)$_2$Ph), 0.75 (t, 6H, ^3J = 7.2 Hz, N(CH$_2$CH_3)$_2$). ^{13}C NMR (CDCl$_3$, 100 MHz): δ 153.9, 153.5, 152.0, 151.9, 139.4, 135.5, 132.9, 131.4, 128.0, 127.8, 127.0, 126.7, 126.0, 125.5, 124.9, 124.7, 123.5, 123.0, 119.0 (all ArC), 57.8 (ArCH$_2$N), 53.5 (ArCH$_2$N), 50.5 (NCH$_2$CH$_2$N), 50.0 (NCH$_2$$CH_2$N), 46.7 (N($CH_3$)$_2$), 45.4 (N($CH_3$)$_2$), 42.7 ($C$(CH$_3$)$_2$Ph), 42.3 ($C$(CH$_3$)$_2$Ph), 31.4 (C($CH_3$)$_2$Ph), 29.7 (C($CH_3$)$_2$Ph), 11.3 (N(CH$_2$$CH_3$)$_2$). Anal. Calcd for C$_{40}H_{53}N_3$O: C, 81.17; H, 9.03; N, 7.10. Found: C, 81.07; H, 9.11; N, 6.70.

4,6-Dicumyl-2-{N-[2-(N′,N′-dimethylamino)benzyl]-N-[2-(N″,N″-diisopropylamino)ethyl]aminomethyl}phenol (L³H). The procedure was the same as that of **L¹H**, except that 2-(dimethylamino)-benzaldehyde (1.9 g, 12 mmol), N,N-diisopropylethane-1,2-diamine (1.8 g, 12 mmol), sodium sulfate (1.9 g, 12 mmol), NaBH$_4$ (0.94 g, 25 mmol), paraformaldehyde (0.45 g, 15 mmol), and 2,4-dicumylphenol (4.1 g, 12 mmol) were used to afford **L³H** as a viscous oil (4.96 g, 64.5%). ^{1}H NMR (CDCl$_3$, 400 MHz): δ 7.27−7.14 (m, 11H, ArH, overlapped with the CDCl$_3$ signal), 7.10 (tt, 1H, ^3J = 6.8 Hz, ^4J = 2.0 Hz, ArH), 7.04 (dd, 1H, ^3J = 8.0 Hz, ^4J = 1.0 Hz, ArH), 6.99 (dd, 1H, ^3J = 7.9 Hz, ^4J = 1.6 Hz, ArH), 6.89 (td, 1H, ^3J = 7.4 Hz, ^4J = 0.8 Hz, ArH), 6.77 (d, 1H, ^4J = 2.4 Hz, ArH), 3.65 (s, 2H, ArCH_2N), 3.59 (s, 2H, ArCH_2N), 2.73 (hept, 2H, ^3J = 6.4 Hz, NCH(CH$_3$)$_2$), 2.56 (s, 6H, N(CH_3)$_2$), 2.32−2.27 (m, 2H, NCH$_2$CH_2N), 2.23−2.18 (m, 2H, NCH_2CH$_2$N), 1.68 (s, 12H, C(CH_3)$_2$Ph), 0.75 (d, 12H, ^3J = 6.4 Hz, NCH(CH_3)$_2$). ^{1}H NMR (C$_6$D$_6$, 400 MHz): δ 10.76 (s, 1H, OH), 7.52 (d, 1H, ^4J = 2.0 Hz, ArH), 7.43 (d, 1H, ^3J = 7.6 Hz, ArH), 7.37 (d, 1H, ^3J = 8.0 Hz, ArH), 7.22−7.17 (m, 4H, ArH), 7.11−7.04 (m, 4H, ArH), 6.89 (m, 2H, ArH), 6.89 (d, 1H, ^4J = 2.0 Hz, ArH), 3.53 (s, 2H, ArCH_2N), 3.43 (s, 2H, ArCH_2N), 2.66 (hept, 2H, ^3J = 6.4 Hz, N[CH(CH$_3$)$_2$]$_2$), 2.31 (s, 6H, ArN(CH_3)$_2$), 2.31−2.09 (m, 2H, NCH$_2$CH_2N), 2.24−2.15 (m, 2H, NCH_2CH$_2$N), 1.85 (s, 6H, Ar(CH_3)$_2$Ph), 1.73 (s, 2H, Ar(CH_3)$_2$Ph), 0.74 (d, 12H, ^3J = 6.4 Hz, N[CH(CH_3)$_2$]$_2$). ^{13}C NMR (CDCl$_3$, 100 MHz): δ 154.0, 153.7, 151.8, 151.7, 139.8, 135.3, 132.5, 131.4, 128.0, 127.8, 127.0, 126.0, 125.5, 125.0, 124.8, 123.6, 122.8, 119.4 (all ArC), 59.6 (ArCH$_2$N), 55.2 (ArCH$_2$N), 54.8 (NCH$_2$CH$_2$N), 49.0 (N[CH(CH$_3$)$_2$]$_2$), 45.3 (N(CH$_3$)$_2$), 42.74 (NCH$_2$$CH_2$N), 42.68 ($C$(CH$_3$)$_2$Ph), 42.3 ($C$(CH$_3$)$_2$Ph), 31.4 (C($CH_3$)$_2$Ph), 29.7 (C($CH_3$)$_2$Ph), 20.6 (N[CH-($CH_3$)$_2$]$_2$). Anal. Calcd for C$_{42}H_{57}N_3$O: C, 81.37; H, 9.27; N, 6.78. Found: C, 81.29; H, 9.21; N, 6.68.

6-Trityl-2-{N-[2-(N′,N′-dimethylamino)benzyl]-N-[2-(N″,N″-diethylamino)ethyl]aminomethyl}-4-methylphenol (L⁴H). The procedure was the same as that of **L¹H**, except that 2-(dimethylamino)-benzaldehyde (2.7 g, 15 mmol), N,N-diethylethane-1,2-diamine (1.7 g, 15 mmol), sodium sulfate (2.3 g, 15 mmol), NaBH$_4$ (0.94 g, 25 mmol), paraformaldehyde (0.45 g, 15 mmol), and 4-methyl-2-tritylphenol (5.3 g, 15 mmol) were used to afford **L⁴H** as a colorless crystalline solid (6.9 g, 72%). ^{1}H NMR (CDCl$_3$, 400 MHz): δ 10.42 (br, 1H, ArOH), 7.25−7.23 (m, 6H, ArH), 7.18 (t, 6H, ^3J = 7.6 Hz, ArH), 7.14−7.10 (m, 4H, ArH), 7.00 (d, 1H, ^3J = 8.0 Hz, ArH), 6.93−6.87 (m, 3H, ArH), 6.84 (br s, 1H, ArH), 3.61 (s, 2H, ArCH_2N), 3.54 (s, 2H, ArCH_2N), 2.57 (s, 6H, N(CH_3)$_2$), 2.29 (br s, 4H, NCH$_2$CH_2N), 2.17 (s, 3H, ArCH_3), 2.16 (q, 4H, ^3J = 7.2 Hz, N(CH_2CH$_3$)$_2$), 0.72 (t, 6H, ^3J = 7.2 Hz, N(CH$_2$CH_3)$_2$). ^{1}H NMR (C$_6$D$_6$, 400 MHz): δ 10.53 (s, 1H, OH), 7.58 (d, 6H, ^3J = 7.6 Hz, ArH), 7.38 (d, 1H, ^4J = 1.2 Hz, ArH), 7.28 (d, 1H, ^3J = 7.4 Hz, ArH), 7.17−7.13 (m, 7H, ArH), 7.10 (d, 1H, ^3J = 7.2 Hz, ArH), 7.05 (t, 3H, ^3J = 7.4 Hz, ArH), 6.91 (d, 1H, ^3J = 7.6 Hz, ArH), 6.86 (d, 1H, ^4J = 1.2 Hz, ArH), 3.70 (s, 2H, ArCH_2N), 3.48 (s, 2H, ArCH_2N), 2.35 (s, 6H, N(CH_3)$_2$), 2.24 (m, 2H, NCH$_2$CH_2N), 2.17 (s, 3H, ArCH_3), 2.09 (m, 2H, NCH_2CH$_2$N), 2.03 (q, 4H, ^3J = 7.0 Hz, N(CH_2CH$_3$)$_2$), 0.70 (t, 6H, ^3J = 7.0 Hz, N(CH$_2$CH_3)$_2$). ^{13}C NMR (CDCl$_3$, 100 MHz): δ

154.1, 153.2, 146.4, 133.7, 132.7, 131.4, 131.0, 130.8, 129.5, 127.4, 127.0, 125.8, 125.2, 123.5, 123.3, 118.5 (all ArC), 63.4 (CPh$_3$), 57.0 (ArCH$_2$N), 52.5 (ArCH$_2$N), 49.8 (NCH$_2$CH$_2$N), 49.5 (NCH$_2$$CH_2$N), 46.4 (N(C$H_3$)$_2$), 45.4 (N(C$H_2CH_3$)$_2$), 21.0 (Ar$CH_3$), 11.1 (N-(CH$_2$$CH_3$)$_2$). Anal. Calcd for C$_{42}H_{49}N_3$O: C, 82.45; H, 8.07; N, 6.87. Found: C, 82.07; H, 8.04; N, 6.71.

6-Trityl-2-{N-[2-(N′,N′-diethylamino)benzyl]-N-[2-(N″,N″-diethylamino)ethyl]aminomethyl}-4-methylphenol (L⁵H). The procedure was the same as that of **L¹H**, except that 2-(diethylamino)-benzaldehyde (3.5 g, 20 mmol), N,N-diethylethane-1,2-diamine (2.3 g, 20 mmol), sodium sulfate (3.1 g, 20 mmol), NaBH$_4$ (1.1 g, 30 mmol), paraformaldehyde (0.6 g, 20 mmol), and 4-methyl-2-tritylphenol (7.1 g, 20 mmol) were used to afford **L⁵H** as a colorless crystalline solid (8.9 g, 73%). ^{1}H NMR (CDCl$_3$, 400 MHz): δ 10.4 (br, 1H, OH), 7.25−7.23 (m, 6H, ArH), 7.18 (t, 6H, ^3J = 7.2 Hz, ArH), 7.13−7.09 (m, 4H, ArH), 7.01 (d, 1H, ^3J = 8.0 Hz, ArH), 6.94−6.89 (m, 3H, ArH), 6.84 (s, 1H, ArH), 3.59 (s, 2H, ArCH_2N), 3.54 (s, 2H, ArCH_2N), 2.89 (q, 4H, ^3J = 7.2 Hz, ArN(CH_2CH$_3$)$_2$), 2.32−2.27 (m, 4H, NCH$_2$CH_2N), 2.17 (s, 3H, ArCH_3), 2.13 (q, 4H, ^3J = 7.2 Hz, N(CH_2CH$_3$)$_2$), 0.92 (t, 6H, ^3J = 7.2 Hz, ArN(CH$_2$CH_3)$_2$), 0.70 (t, 6H, ^3J = 7.2 Hz, N(CH$_2$CH_3)$_2$). ^{1}H NMR (C$_6$D$_6$, 400 MHz): δ 10.54 (s, 1H, OH), 7.57 (d, 6H, ^3J = 7.2 Hz, ArH), 7.36 (s, 1H, ArH), 7.29 (dd, 1H, ^3J = 6.8 Hz, ^4J = 1.6 Hz, ArH), 7.15−7.08 (m, 7H, ArH, overlapped with the C$_6$D$_6$ signal), 7.04 (t, 4H, ^3J = 7.2 Hz, ArH), 6.92 (dd, 1H, ^3J = 7.6 Hz, ^4J = 1.6 Hz, ArH), 6.86 (s, 1H, ArH), 3.73 (s, 2H, ArCH_2N), 3.48 (s, 2H, ArCH_2N), 2.72 (q, 4H, ^3J = 7.2 Hz, ArN(CH_2CH$_3$)$_2$), 2.26 (br, 2H, NCH$_2$CH_2N), 2.14 (s, 3H, ArCH_3), 2.12 (br, 2H, NCH_2CH$_2$N), 2.01 (q, 4H, ^3J = 7.2 Hz, N(CH_2CH$_3$)$_2$), 0.83 (t, 6H, ^3J = 7.2 Hz, ArN(CH$_2$CH_3)$_2$), 0.67 (t, 6H, ^3J = 7.2 Hz, N(CH$_2$CH_3)$_2$). ^{13}C NMR (CDCl$_3$, 100 MHz): δ 154.1, 150.0, 146.4, 135.5, 133.7, 131.4, 130.9, 130.8, 129.6, 127.0, 126.8, 125.8, 125.2, 123.8, 123.5, 122.0 (all ArC), 63.5 (CPh$_3$), 57.0 (ArCH$_2$N), 52.1 (ArCH$_2$N), 49.8 (NCH$_2$CH$_2$N), 49.6 (NCH$_2$$CH_2$N), 48.3 (ArN-($CH_2CH_3$)$_2$), 46.2 (N($CH_2CH_3$)$_2$), 21.0 (Ar$CH_3$), 12.4 (ArN-(CH$_2$$CH_3$)$_2$), 11.0 (N(CH$_2$$CH_3$)$_2$). Anal. Calcd for C$_{44}H_{53}N_3$O: C, 82.59; H, 8.35; N, 6.57. Found: C, 82.50; H, 8.29; N, 6.46.

4,6-Dicumyl-2-{N-[2-(N′,N′-dimethylamino)benzyl]-N-[(S)-1-(n-butylpyrrolidin-2-yl)methyl]aminomethyl}phenol (L⁶H). (S)-(1-n-Butylpyrrolidin-2-yl)methanamine (2.3 g, 15 mmol) was added to a solution of 2-(dimethylamino)benzaldehyde (2.2 g, 15 mol) in ethanol (20 mL), and the mixture was heated to reflux for 24 h. After cooling to room temperature, NaBH$_4$ (1.1 g, 30 mmol) was added sequentially to the above light-yellow solution three times, and the mixture was stirred for 3 h at 50 °C. The mixture was poured into water (80 mL) and extracted with CH$_2$Cl$_2$ (3 × 50 mL). The organic phase was dried over anhydrous MgSO$_4$. Evaporation of the solvent afforded (S)-N-(2′-N′,N′-dimethylamino)benzyl-1-(1-n-butylpyrrolidin-2-yl)-methanamine as a viscous oil (4.3 g, ∼90% purity), which was used directly for the next step without further purification. Paraformaldehyde (0.676 g, 22.5 mmol) and 2,4-dicumylphenol (4.96 g, 15.0 mmol) were added to a solution of (S)-N-(2′-N′,N′-dimethylamino)-benzyl-1-(1-n-butylpyrrolidin-2-yl)methanamine (4.3 g) in ethanol (30 mL) at 90 °C during 12 h with stirring. The mixture was cooled to ambient temperature and concentrated under vacuum to give a yellow oil, which was purified by column chromatography (Merck silica gel 100; petroleum ether:ethyl acetate = 5:1) to provide a light-yellow viscous oil (4.6 g, 49%) after removal of all of the volatiles. ^{1}H NMR (400 MHz, CDCl$_3$): δ 10.26 (s, 1H, OH), 7.27−7.26 (m, 4H, ArH, overlapped with the CDCl$_3$ signal), 7.21−7.15 (m, 7H, ArH), 7.11−7.07 (m, 1H, ArH), 7.04 (d, 1H, ^3J = 7.6 Hz, ArH), 6.95 (dd, 1H, ^3J = 7.6 Hz, ^4J = 1.6 Hz, ArH), 6.89 (t, 1H, ^3J = 7.2 Hz, ArH), 6.75 (d, 1H, ^4J = 1.2 Hz, ArH), 3.78 (d, 1H, ^2J = 13.6 Hz, ArCH_2N), 3.68 (d, 1H, ^2J = 12.8 Hz, ArCH_2N), 3.47 (d, 1H, ^2J = 12.8 Hz, ArCH_2N), 3.40 (d, 1H, ^2J = 13.6 Hz, ArCH_2N), 3.00−2.97 (m, 1H, NCH− of pyrrolidinyl), 2.56 (s, 6H, N(CH_3)$_2$), 2.53−2.48 (m, 1H, NCH_2− of pyrrolidinyl), 2.40 (d, 1H, ^3J = 11.6 Hz, NCH_2CH), 2.31−2.20 (m, 2H, NCH$_2$CH and NCH_2− of pyrrolidinyl), 1.96−1.90 (m, 2H, NCH$_2$CH_2CH$_2$CH$_3$), 1.68 (s, 9H, C(CH_3)$_2$Ph), 1.63 (s, 3H, C(CH_3)$_2$Ph), 1.60−1.16 (m, 7H, −CH_2− of pyrrolidinyl and NCH$_2$CH_2CH_2CH$_3$), 1.05−0.98 (m, 1H, NCH$_2$CH$_2$CH$_2$CH_3), 0.88

(t, 3H, ^3J = 7.2 Hz, N(CH$_2$)$_3$CH_3). ^{1}H NMR (C$_6$D$_6$, 400 MHz): δ 10.77 (s, 1H, OH), 7.53 (d, 1H, ^4J = 2.0 Hz, ArH), 7.43 (d, 2H, ^3J = 7.6 Hz, ArH), 7.36 (d, 2H, ^3J = 7.6 Hz, ArH), 7.21−7.15 (m, 4H, ArH, overlapped with the C$_6$D$_6$ signal), 7.07 (t, 4H, ^3J = 7.4 Hz, ArH), 6.93 (d, 1H, ^3J = 7.2 Hz, ArH), 6.89 (d, 1H, ^3J = 2.0 Hz, ArH), 6.88 (t, 1H, ^3J = 8.0 Hz, ArH), 3.59 (d, 1H, ^2J = 13.6 Hz, ArCH_2N), 3.58 (d, 1H, ^2J = 12.4 Hz, NCH_2Ar), 3.52 (d, 1H, ^2J = 12.4 Hz, NCH_2Ar), 3.30 (d, 1H, ^2J = 13.6 Hz, ArCH_2N), 2.89−2.85 (m,1H, NCH− of pyrrolidinyl), 2.52−2.45 (m, 1H, NCH_2− of pyrrolidinyl), 2.41−2.32 (m, 2H, NCH_2CH$_2$CH$_2$CH$_3$), 2.30 (s, 6H, ArN(CH_3)$_2$), 2.21−2.12 (m, 1H, NCH_2− of pyrrolidinyl), 1.91−1.88 (m, 1H, NCH$_2$CH), 1.88 (s, 3H, C(CH_3)$_2$Ph), 1.82 (s, 3H, C(CH_3)$_2$Ph), 1.77−1.72 (m, 1H, NCH$_2$CH), 1.72 (s, 3H, C(CH_3)$_2$Ph), 1.72 (s, 3H, C(CH_3)$_2$Ph), 1.54 (m, 1H, −CH_2− of pyrrolidinyl and NCH_2(CH$_2$)$_2$CH$_3$), 1.15−1.04 (m, 1H, NCH_2(CH$_2$)$_2$CH$_3$), 0.87 (t, 3H, ^3J = 6.8 Hz, NCH$_2$(CH$_2$)$_2$CH_3). ^{13}C NMR (CDCl$_3$, 100 MHz): δ 153.7, 153.6, 151.6, 151.4, 139.7, 135.1, 132.2, 131.6, 128.1, 127.9, 127.6, 126.9, 126.0, 125.9, 125.4, 124.8, 124.6, 123.5, 122.4, 119.4 (all ArC), 62.6 (ArCH$_2$N), 60.1 (NCH$_2$Ar), 58.9 (NCH− of pyrrolidinyl), 55.4 (NCH$_2$CH), 55.0 (NCH$_2$− of pyrrolidinyl), 54.3 (NCH$_2$CH$_2$CH$_2$CH$_3$), 45.4 (ArN(CH$_3$)$_2$), 42.6 (C(CH$_3$)$_2$Ph), 42.0 (C(CH$_3$)$_2$Ph), 31.3 (C(CH$_3$)$_2$Ph), 31.2 (C(CH$_3$)$_2$Ph), 31.1 (C(CH$_3$)$_2$Ph), 30.1 (C(CH$_3$)$_2$Ph), 30.0 (N CH$_2$$CH_2CH_2CH_3$), 28.9 (−$CH_2$− of pyrrolidinyl), 22.7 (−CH$_2$− of pyrrolidinyl), 21.0 (NCH$_2$$CH_2CH_2CH_3$), 14.2 (NCH$_2CH_2CH_2$$CH_3$). Anal. Calcd for C$_{43}H_{57}N_3$O·0.3C$_6H_{14}$: C, 81.80; H, 9.38; N, 6.39. Found: C, 81.80; H, 9.52; N, 6.34.

6-Trityl-2-{N-[2-(N′,N′-dimethylamino)benzyl-N-[(S)-(1-n-butyl-pyrrolidin-2-yl)methyl]aminomethyl}-4-methylphenol (L⁷H). The procedure was the same as that of **L⁶H**, except that (S)-(1-n-butylpyrrolidin-2-yl)methanamine (3.8 g, 20 mmol), NaBH$_4$ (1.1 g, 30 mmol), paraformaldehyde (0.676 g, 22.5 mmol), and 4-methyl-2-tritylphenol (7.0 g, 20 mmol) were used to afford **L⁷H** as a colorless crystalline solid (5.5 g, 56%). ^{1}H NMR (CDCl$_3$, 400 MHz): δ 10.36 (s, 1H, OH), 7.23−7.15 (m, 13H, ArH), 7.14−7.09 (m, 3H, ArH), 7.00 (d, 1H, ^3J = 7.6 Hz, ArH), 6.89 (d, 1H, ^4J = 1.6 Hz, ArH), 6.87 (dd, 1H, ^3J = 7.2 Hz, ^4J = 0.8 Hz, ArH), 6.84 (dd, 1H, ^3J = 7.6 Hz, ^4J = 1.6 Hz, ArH), 6.78 (d, 1H, ^4J = 1.6 Hz, ArH), 3.79 (d, 1H, ^2J = 13.5 Hz, ArCH_2N), 3.63 (d, 1H, ^2J = 12.9 Hz, ArCH_2N), 3.50 (d, 1H, ^2J = 13.5 Hz, ArCH_2N), 3.45 (d, 1H, ^2J = 12.9 Hz, ArCH_2N), 2.93−2.90 (m, 1H, NCH− of pyrrolidinyl), 2.52 (s, 6H, N(CH_3)$_2$), 2.50−2.42 (m, 1H, NCH_2− of pyrrolidinyl), 2.35 (m, 1H, NCH$_2$CH), 2.25−2.11 (m, 2H, NCH_2CH$_2$CH$_2$CH$_3$), 2.16 (s, 3H, PhCH_3), 1.91−1.82 (m, 2H, NCH$_2$CH and NCH_2− of pyrrolidinyl), 1.51−1.36 (m, 3H, −CH_2− of pyrrolidinyl), 1.35−1.12 (m, 4H, NCH$_2$CH_2CH_2CH$_3$), 0.97−0.88 (m, 1H, −CH_2− of pyrrolidinyl), 0.84 (t, 3H, ^3J = 7.2 Hz, N(CH$_2$)$_3$CH_3). ^{1}H NMR (C$_6$D$_6$, 400 MHz): δ 10.75 (s, 1H, OH), 7.56 (d, 6H, ^3J = 7.6 Hz, ArH), 7.35 (s, 1H, ArH), 7.14−7.08 (m, 11H, ArH), 7.05−6.96 (m, 1H, ArH), 6.88 (d, 1H, ^3J = 8.0 Hz, ArH), 6.77 (s, 1H, ArH), 3.72 (d, 1H, ^2J = 13.6 Hz, ArCH_2N), 3.68 (d, 1H, ^2J = 12.8 Hz, NCH_2Ar), 3.59 (d, 1H, ^2J = 12.8 Hz, NCH_2Ar), 3.48 (d, 1H, ^2J = 13.6 Hz, ArCH_2N), 2.83 (m, 1H, NCH− of pyrrolidinyl), 2.46 (m, 1H, NCH_2− of pyrrolidinyl), 2.42−2.32 (m, 2H, NCH_2(CH$_2$)$_2$CH$_3$), 2.31 (s, 6H, ArN(CH_3)$_2$), 2.13 (s, 3H, ArCH_3), 2.13−2.08 (m, 1H, NCH_2− of pyrrolidinyl), 1.87−1.78 (m, 1H, NCH$_2$CH), 1.75−1.69 (m, 1H, NCH$_2$CH), 1.49−1.39 (m, 1H, −CH_2− of pyrrolidinyl), 1.36−1.14 (m, 6H, −CH_2− of pyrrolidinyl and NCH$_2$(CH_2)$_2$CH$_3$), 1.12−1.04 (m, 1H, NCH$_2$CH_2CH$_2$CH$_3$), 0.84 (t, 1H, ^3J = 6.8 Hz, NCH$_2$(CH$_2$)$_2$CH_3). ^{13}C NMR (CDCl$_3$, 100 MHz): δ 154.1, 153.5, 146.3, 133.5, 132.0, 131.6, 131.4, 130.7, 129.0, 127.9, 127.0, 126.3, 125.3, 123.4, 123.1, 119.0 (all ArC), 63.4 (CPh$_3$), 62.7 (ArCH$_2$N), 60.0 (ArCH$_2$N), 58.1 (NCH− of pyrrolidinyl), 55.2 (NCH$_2$CH), 54.3 (NCH$_2$− of pyrrolidinyl), 54.2 (NCH$_2$CH$_2$CH$_2$CH$_3$), 45.3 (N(CH$_3$)$_2$), 31.0 (NCH$_2$$CH_2CH_2CH_3$), 29.9 (−$CH_2$− of pyrrolidinyl), 22.7 (−CH$_2$− of pyrrolidinyl), 21.0 (ArCH$_3$), 20.9 (NCH$_2$CH$_2$$CH_2CH_3$), 14.2 (NCH$_2CH_2CH_2$$CH_3$). Anal. Calcd for C$_{45}H_{53}N_3$O: C, 82.91; H, 8.19; N, 6.45. Found: C, 82.88; H, 8.23; N, 6.36.

[(L¹)ZnN(SiMe₃)₂] (1). In a glovebox, a solution of proligand **L¹H** (0.679 g, 1.50 mmol) in toluene (2 mL) was cannulated to a solution

of Zn[N(SiMe$_3$)$_2$]$_2$ (0.579 g, 1.50 mmol) in toluene. The reaction mixture was allowed to be stirred at room temperature overnight. The solvent and volatile components were removed under reduced pressure to afford a light-yellow vesicular solid. After recrystallization with n-hexane, colorless crystals were isolated in 49.2% yield (0.500 g). ^{1}H NMR (C$_6$D$_6$, 400 MHz): δ 7.50 (d, 1H, ^4J = 2.4 Hz, ArH), 6.86 (td, 1H, ^3J = 8.0 Hz, ^4J = 1.2 Hz, ArH), 6.76 (t, 1H, ^3J = 8.0 Hz, ArH), 6.69−6.67 (m, 2H, ArH), 6.55 (d, 1H, ^3J = 8.0 Hz, ArH), 4.44 (d, 1H, ^2J = 12.4 Hz, NCH_2Ar), 3.76 (d, 1H, ^2J = 14.0 Hz, NCH_2Ar), 3.10−3.01 (m, 1H, NCH_2CH$_2$N), 2.93 (d, 1H, ^2J = 12.4 Hz, NCH_2Ar), 2.78 (hept, 2H, ^3J = 6.4 Hz, CH(CH$_3$)$_2$), 2.73−2.59 (m, 2H, NCH_2CH$_2$N), 2.53 (s, 3H, ArN(CH_3)$_2$), 2.51 (d, 1H, ^2J = 14.0 Hz, NCH_2Ar), 2.48−2.42 (m, 1H, NCH_2CH$_2$N), 2.12 (s, 3H, ArN(CH_3)$_2$), 0.93 (d, 6H, ^3J = 6.4 Hz, NCH(CH_3)$_2$), 0.91 (d, 6H, ^3J = 6.4 Hz, CH(CH_3)$_2$), 0.64 (br s, 9H, N[Si(CH_3)$_3$]$_2$), 0.01 (br s, 9H, N[Si(CH_3)$_3$]$_2$). ^{13}C NMR (C$_6$D$_6$, 100 MHz): δ 161.8, 149.6, 134.0, 130.7, 130.4, 129.9, 128.7, 126.4, 125.5, 123.0, 120.3, 116.8 (all ArC), 59.6 (ArCH$_2$N), 57.8 (ArCH$_2$N), 55.3 (NCH$_2$CH$_2$N), 49.1 (NCH(CH$_3$)$_2$), 49.0 (NCH(CH$_3$)$_2$), 46.6 (NCH$_2$CH$_2$N), 37.8 (ArN(CH$_3$)$_2$), 21.7 (NCH(CH_3)$_2$), 20.8 (NCH(CH_3)$_2$), 6.7 (N[Si(CH_3)$_3$]), 6.3 (N[Si(CH_3)$_3$]). Anal. Calcd for C$_{30}$H$_{52}$Cl$_2$N$_4$OSi$_2$Zn: C, 53.20; H, 7.74; N, 8.27. Found: C, 53.19; H, 7.74; N, 8.26.

[(L²)ZnN(SiMe₃)₂] (2). The procedure was the same as that of complex **1**, except that **L²H** (1.18 g, 2.00 mmol) and Zn[N(SiMe$_3$)$_2$]$_2$ (0.772 g, 2.00 mmol) were used to afford complex **2** as a white solid (0.750 g, 46%). ^{1}H NMR (C$_6$D$_6$, 400 MHz): δ 7.58 (d, 3H, ^3J = 7.2 Hz, ArH), 7.29 (br, 2H, ArH), 7.18−7.13 (m, 3H, ArH, overlapped with the C$_6$D$_6$ signal), 7.04−6.95 (m, 4H, ArH), 6.86−6.73 (m, 4H, ArH), 4.44 (d, 1H, ^2J = 12.4 Hz, ArCH_2N), 4.36−4.14 (br, 1H, ArCH_2N), 4.10−4.01 (br, 1H, ArCH_2N), 3.33 (br, 1H, ArCH_2N), 2.45−1.64 (br m, 26H, N(CH_2CH$_3$)$_2$, NCH_2CH$_2$N, N(CH_3)$_2$, C(CH_3)$_2$Ph), 0.81−0.05 (very br, 6H, N(CH$_2$CH_3)$_2$, overlapped with the resonance of N[Si(CH_3)$_3$]$_2$), 0.51 (br s, 18H, N[Si(CH_3)$_3$]$_2$). ^{13}C NMR (C$_6$D$_6$, 100 MHz): δ (fluxional) 165.3, 152.9, 152.2, 137.4, 134.1, 133.4, 130.1, 128.9, 127.9, 127.4, 127.2, 125.5, 124.6, 121.6, 120.4 (all ArC), 60.4 (ArCH$_2$N), 53.6 (NCH$_2$Ar), 49.8 (br, NCH$_2$CH$_2$N), 45.9 (NCH$_2$CH$_2$N), 43.9 (N(CH$_2$CH$_3$)$_2$), 42.8 (N(CH$_3$)$_2$), 42.4 (C(CH$_3$)$_2$Ph), 34.4 (H$_3$)Ph), 31.5 (C(CH$_3$)$_2$Ph), 31.4 (C(CH$_3$)$_2$Ph), 26.4 (C(CH$_3$)$_2$Ph), 23.1 (C(CH$_3$)$_2$Ph), 14.4 (N(CH$_2$$CH_3$)$_2$), 7.4 (N[Si(C$H_3$)$_3$]$_2$). Anal. Calcd for C$_{46}H_{70}N_4OSi_2$Zn: C, 67.65; H, 8.64; N, 6.86. Found: C, 67.48; H, 8.47; N, 6.76.

[(L³)ZnN(SiMe₃)₂] (3). The procedure was the same as that of complex **1**, except that **L³H** (1.30 g, 2.10 mmol) and Zn[N(SiMe$_3$)$_2$]$_2$ (0.812 g, 2.10 mmol) were used to afford complex **3** as colorless crystals (0.840 g, 47.3%). ^{1}H NMR (C$_6$D$_6$, 400 MHz): δ 7.74 (d, 1H, ^4J = 2.8 Hz, ArH), 7.65 (d, 2H, ^3J = 7.2 Hz, ArH), 7.45 (dd, 2H, ^3J = 8.4 Hz, ArH), 7.20−7.12 (m, 4H, ArH), 7.04 (tt, 1H, ^3J = 7.2 Hz, ^4J = 1.2 Hz, ArH), 7.01−6.95 (m, 2H, ArH), 6.85 (td, 1H, ^3J = 7.6 Hz, ^4J = 1.2 Hz, ArH), 6.74 (t, 1H, ^3J = 7.6 Hz, ArH), 6.69 (dd, 1H, ^3J = 7.6 Hz, ^4J = 1.6 Hz, ArH), 6.53 (d, 1H, ^3J = 8.0 Hz, ArH), 4.54 (d, 1H, ^2J = 12.4, ArCH_2N), 4.26 (d, 1H, ^2J = 14.0, ArCH_2N), 3.43 (d, 1H, ^2J = 12.4, ArCH_2N), 2.88 (d, 1H, ^2J = 14.0, ArCH_2N), 2.74 (hept, 2H, ^3J = 6.4 Hz, N[CH(CH$_3$)$_2$]$_2$), 2.63−2.46 (m, 4H, NCH_2CH$_2$N), 2.31 (br, 3H, N(CH_3)$_2$), 2.24 (s, 3H, C(CH_3)$_2$Ph), 1.84 (s, 6H, C(CH_3)$_2$Ph), 1.76 (s, 3H, C(CH_3)$_2$Ph), 1.26 (br, 3H, N(CH_3)$_2$), 0.85 (d, 6H, ^3J = 6.4 Hz, N[CH(CH_3)$_2$]$_2$), 0.85 (d, 6H, ^3J = 6.4 Hz, N[CH(CH_3)$_2$]$_2$), 0.70−0.20 (br, 9H, N[Si(CH_3)$_3$]$_2$), 0.50−0.20 (br, 9H, N[Si(CH_3)$_3$]$_2$). ^{13}C NMR (C$_6$D$_6$, 100 MHz): δ 165.0, 152.6, 152.2, 150.2, 137.3, 134.0, 133.6, 130.2, 129.4, 129.1, 128.2, 127.9, 127.6, 127.3, 126.0, 125.7, 124.9, 120.1, 120.0 (all ArC), 61.0 (ArCH$_2$N), 56.6 (ArCH$_2$N), 53.8 (NCH$_2$CH$_2$N), 49.3 (ArN(CH$_3$)$_2$), 49.0 (N[CH(CH$_3$)$_2$]$_2$), 45.4 (ArN(CH$_3$)$_2$), 42.7 (C(CH$_3$)$_2$Ph), 42.6 (C(CH$_3$)$_2$Ph), 36.0 (NCH$_2$CH$_2$N), 34.5 (C(CH$_3$)$_2$Ph), 31.9 (C(CH$_3$)$_2$Ph), 31.8 (C(CH$_3$)$_2$Ph), 26.1 (C(CH$_3$)$_2$Ph), 21.4 (N[CH(CH_3)$_2$]$_2$), 21.0 (N[CH(CH_3)$_2$]$_2$), 6.9 (N[Si(CH_3)$_3$]$_2$). Anal. Calcd for C$_{48}$H$_{74}$N$_4$OSi$_2$Zn: C, 68.25; H, 8.83; N, 6.63. Found: C, 67.71; H, 8.91; N, 6.45.

[(L⁴)ZnN(SiMe₃)₂] (4). A procedure similar to that of complex **1** was adopted, except that **L⁴H** (0.640 g, 1.00 mmol) and Zn[N(SiMe$_3$)$_2$]$_2$

(0.386 g, 1.00 mmol) were used to afford complex **4** as colorless crystals (0.450 g, 52.0%) after recrystallization with a mixture of toluene and *n*-hexane. ^{1}H NMR (C$_6$D$_6$, 400 MHz): δ 7.69 (d, 6H, ^3J = 5.6 Hz, Ar*H*), 7.59 (d, 1H, ^3J = 7.6 Hz, Ar*H*), 7.48–7.42 (br, 1H, Ar*H*), 7.14–7.08 (m, 7H, Ar*H*), 6.97–6.85 (m, 5H, Ar*H*), 6.53–6.32 (br, 1H, Ar*H*), 4.64–4.29 (br, 2H, ArC*H$_2$*N), 4.28–3.89 (br, 1H, ArC*H$_2$*N), 3.44–3.09 (br, 1H, ArC*H$_2$*N), 2.11–2.10 (m, 17H, NC*H$_2$*C*H$_2$*N, ArC*H$_3$*, ArN(C*H$_3$*)$_2$, N(CH$_2$C*H$_3$*)$_2$), 0.63–0.03 (very br, 6H, N(C*H$_2$*CH$_3$)$_2$, overlapped with the resonance of N[Si-(C*H$_3$*)$_3$]$_2$), 0.36 (s, 18H, N[Si(C*H$_3$*)$_3$]$_2$). ^{1}H NMR (toluene-*d$_8$*, 400 MHz, 223 K): δ 8.45 (br, 1H, Ar*H*), 7.90 (br, 1H, Ar*H*), 7.59 (br, 1H, Ar*H*), 7.44 (s, 1H, Ar*H*), 7.33–7.24 (m, 4H, Ar*H*), 7.19 (d, 1H, ^3J = 4.4 Hz, Ar*H*), 7.11–7.06 (m, 2H, Ar*H*, overlapped with the toluene-*d$_8$* signal), 7.00–6.89 (m, 6H, Ar*H*, overlapped with the toluene-*d$_8$* signal), 6.85 (d, 2H, ^3J = 4.8 Hz, Ar*H*), 6.75 (d, 1H, ^3J = 4.0 Hz, Ar*H*), 6.25 (s, 1H, Ar*H*), 4.48 (d, 1H, ^2J = 9.2 Hz, ArC*H$_2$*N), 4.30 (d, 1H, ^2J = 8.0 Hz, ArC*H$_2$*N), 3.96 (d, 1H, ^2J = 9.2 Hz, ArC*H$_2$*N), 3.14 (d, 1H, ^2J = 8.0 Hz, ArC*H$_2$*N), 2.47–2.41 (m, 2H, NC*H$_2$*CH$_2$N), 2.32–2.23 (m, 2H, NC*H$_2$*CH$_2$N), 2.23 (br s, 6H, ArN(C*H$_3$*)$_2$), 2.07–2.02 (m, 1H, N(C*H$_2$*CH$_3$)$_2$, overlapped with the toluene-*d$_8$* signal), 2.02 (s, 3H, ArC*H$_3$*), 1.80–1.78 (m, 2H, N(C*H$_2$*CH$_3$)$_2$), 1.10–1.04 (m, 1H, N(C*H$_2$*CH$_3$)$_2$), 0.83 (t, 3H, ^3J = 4.0 Hz, N(CH$_2$C*H$_3$*)$_2$), 0.38 (s, 18H, N[Si(C*H$_3$*)$_3$]$_2$), −0.32 (t, 3H, ^3J = 4.0 Hz, N(CH$_2$C*H$_3$*)$_2$). ^{13}C NMR (C$_6$D$_6$, 100 MHz): δ (fluxional) 166.1, 147.7, 137.9, 134.52, 132.7, 132.0, 128.6, 128.2, 127.9, 125.7, 124.92, 121.3, 120.3 (all Ar*C*), 64.4 (*C*Ph$_3$), 59.6 (Ar*C*H$_2$N), 52.9 (N*C*H$_2$N), 49.4 (N*C*H$_2$CH$_2$N), 46.0 (NCH$_2$*C*H$_2$N), 32.0 (ArN(*C*H$_3$)$_2$), 21.4 (N(CH$_2$*C*H$_3$)$_2$), 20.8 (N(*C*H$_2$CH$_3$)$_2$), 7.4 (N[Si(*C*H$_3$)$_3$]$_2$). Anal. Calcd for C$_{48}$H$_{66}$N$_4$OSi$_2$Zn·0.5C$_7$H$_8$: C, 70.07; H, 7.99; N, 6.35. Found: C, 69.87; H, 8.02; N, 6.28.

[(L^5)ZnN(SiMe$_3$)$_2$] (5). A procedure similar to that of complex **1** was adopted, except that **L^{5}H** (0.949 g, 1.55 mmol) and Zn[N(SiMe$_3$)$_2$]$_2$ (0.599 g, 1.55 mmol) were used to afford complex **5** as colorless crystals (0.620 g, 47.8%) after recrystallization with a mixtue of toluene and *n*-hexane. ^{1}H NMR (C$_6$D$_6$, 400 MHz): δ 7.70–7.64 (br s, 6H, Ar*H*), 7.43 (d, 1H, ^4J = 1.6 Hz, Ar*H*), 7.18–7.16 (m, 1H, Ar*H*, overlapped with the C$_6$D$_6$ signal), 7.12 (t, 6H, ^3J = 7.6 Hz, Ar*H*, overlapped with the C$_6$D$_6$ signal), 7.01–6.97 (m, 3H, Ar*H*), 6.93 (t, 3H, ^3J = 7.6 Hz, Ar*H*), 6.43 (d, 1H, ^4J = 1.6 Hz, Ar*H*), 4.49 (d, 1H, ^2J = 12.0 Hz, NC*H$_2$*Ar), 4.34 (d, 1H, ^2J = 13.6 Hz, NC*H$_2$*Ar), 4.31 (d, 1H, ^2J = 13.6 Hz, NC*H$_2$*Ar), 3.24 (d, 1H, ^2J = 12.0 Hz, NC*H$_2$*Ar), 2.85–2.72 (m, 4H, ArN(C*H$_2$*CH$_3$)$_2$), 2.50–2.42 (m, 3H, NC*H$_2$*CH$_2$N), 2.06 (s, 3H, ArC*H$_3$*), 1.92–1.88 (m, 1H, NC*H$_2$*CH$_2$N), 0.82 (t, 6H, ^2J = 7.0 Hz, ArN(CH$_2$C*H$_3$*)$_2$), 0.39 (s, 18H, N[Si(C*H$_3$*)$_3$]$_2$); 10 protons attributed to the ethyl groups of the N(CH$_2$C*H$_3$*)$_2$ unit were "disappeared" in the whole spectrum. ^{13}C NMR (C$_6$D$_6$, 100 MHz): δ 166.1, 153.0, 134.8, 134.7, 134.6, 132.6, 132.0, 129.5, 129.2, 128.0, 127.6, 124.9, 124.3, 124.3, 121.4, 120.3 (all Ar*C*), 64.4 (Ar*C*Ph$_3$), 59.6 (Ar*C*H$_2$N), 53.2 (N*C*H$_2$Ar), 49.9 (N*C*H$_2$CH$_2$N), 48.0 (N*C*H$_2$CH$_2$N), 42.9 (N(*C*H$_2$CH$_3$)$_2$), 32.0 (ArN(*C*H$_3$)$_2$), 23.1 (N(CH$_2$*C*H$_3$)$_2$), 20.8 (Ar*C*H$_3$), 14.4 (ArN-(CH$_2$*C*H$_3$)$_2$), 11.6 (N(CH$_2$*C*H$_3$)$_2$), 7.4 (N[Si(*C*H$_3$)$_3$]$_2$). Anal. Calcd for C$_{50}$H$_{70}$N$_4$OSi$_2$Zn·(1.0 C$_6$H$_{14}$): C, 70.73; H, 8.90; N, 5.89. Found: C, 70.35; H, 8.67; N, 5.62.

[(L^6)ZnN(SiMe$_3$)$_2$] (6). The procedure was the same as that of complex **1**, except that **L^{6}H** (0.632 g, 1.00 mmol) and Zn[N-(SiMe$_3$)$_2$]$_2$ (0.386 g, 1.00 mmol) were used to afford complex **6** as a white solid (0.350 g, 40.8%) as a mixture of two diastereomers in a 10:1 molar ratio. Because of the relatively small percentages in the mixture, the NMR signals of minor isomer could not be identified completely; thus, only the NMR spectroscopic data of the major isomer were listed. ^{1}H NMR of the major isomer (C$_6$D$_6$, 400 MHz): δ 7.57–7.56 (m, 3H, Ar*H*), 7.29 (dd, 2H, ^3J = 8.0 Hz, ^4J = 1.2 Hz, Ar*H*), 7.20 (d, 2H, ^3J = 7.6 Hz, Ar*H*), 7.17–7.12 (m, 2H, Ar*H*), 1.08–7.00 (m, 3H, Ar*H*), 6.90 (d, 1H, ^3J = 8.0 Hz, Ar*H*), 6.80 (d, 2H, ^3J = 4.0 Hz, Ar*H*), 6.72 (d, 1H, ^4J = 2.4 Hz, Ar*H*), 4.62 (d, 1H, ^2J = 14.0 Hz, ArC*H$_2$*N), 4.43 (d, 1H, ^2J = 12.4 Hz, NC*H$_2$*Ar), 3.98 (d, 1H, ^2J = 14.0 Hz, ArC*H$_2$*N), 3.44 (d, 1H, ^2J = 12.4 Hz, NC*H$_2$*Ar), 3.45–3.40 (m, 1H, NC*H*− of pyrrolidinyl), 2.35–2.26 (m, 1H, NC*H$_2$*− of pyrrolidinyl), 2.22 (s, 3H, C(C*H$_3$*)$_2$Ph), 2.19 (s, 6H, N(C*H$_3$*)$_2$), 2.11–2.05 (m, 1H,

NC*H$_2$*− of pyrrolidinyl), 1.98−1.80 (m, 4H, NC*H$_2$*CH and NCH$_2$C*H$_2$*CH$_2$CH$_3$), 1.84−1.81 (m, 1H, −C*H$_2$*− of pyrrolidinyl), 1.70 (s, 3H, C(C*H$_3$*)$_2$Ph), 1.64 (s, 3H, C(C*H$_3$*)$_2$Ph), 1.56 (s, 3H, C(C*H$_3$*)$_2$Ph), 1.56−1.47 (m, 2H, −C*H$_2$*− of pyrrolidinyl), 1.31−1.19 (m, 2H, NCH$_2$C*H$_2$*CH$_2$CH$_3$), 1.17−1.09 (m, 2H, NCH$_2$CH$_2$C*H$_2$*CH$_3$), 1.02 (t, 3H, ^3J = 7.2 Hz, NCH$_2$CH$_2$CH$_2$C*H$_3$*), 0.62−0.56 (m, 1H, −C*H$_2$*− of pyrrolidinyl), 0.53 (s, 18H, N[Si-(C*H$_3$*)$_3$]$_2$). ^{13}C NMR (C$_6$D$_6$, 100 MHz): δ 164.4, 155.3, 152.8, 152.7, 137.7, 134.6, 133.4, 130.1, 128.8, 128.2, 127.9, 127.4, 127.1, 125.5, 124.8, 124.4, 121.5, 120.0 (all Ar*C*), 63.9 (Ar*C*H$_2$N), 60.3 (N*C*H$_2$Ar), 56.0 (N*C*H− of pyrrolidinyl), 52.4 (N*C*H$_2$− of pyrrolidinyl), 50.0 (N*C*H$_2$CH), 48.7 (N*C*H$_2$CH$_2$CH$_2$CH$_3$), 45.9 (N(*C*H$_3$)$_2$), 42.9 (*C*(CH$_3$)$_2$Ph), 42.3 (C(*C*H$_3$)$_2$Ph), 34.1 (C(*C*H$_3$)$_2$Ph), 31.5 (C-(*C*H$_3$)$_2$Ph), 31.3 (C(*C*H$_3$)$_2$Ph), 30.8 (NCH$_2$*C*H$_2$CH$_2$CH$_3$), 26.4 (*C*(CH$_3$)$_2$Ph), 24.9 (−*C*H$_2$− of pyrrolidinyl), 20.9 (−*C*H$_2$− of pyrrolidinyl), 19.9 (NCH$_2$CH$_2$*C*H$_2$CH$_3$), 14.3 (NCH$_2$CH$_2$CH$_2$*C*H$_3$), 7.4 (N[Si(*C*H$_3$)$_3$]$_2$). Anal. Calcd for C$_{30}$H$_{52}$Cl$_2$N$_4$OSi$_2$Zn: C, 68.70; H, 8.71; N, 6.54. Found: C, 68.48; H, 9.07; N, 6.65.

[(L^7)ZnN(SiMe$_3$)$_2$] (7). A procedure similar to that of complex **1** was adopted, except that **L^{7}H** (0.978 g, 1.50 mmol) and Zn[N(SiMe$_3$)$_2$]$_2$ (0.579 g, 1.50 mmol) were used to afford complex **7** as a white solid (0.640 g, 48.7%) after recrystallization with a mixture of toluene and *n*-hexane. ^{1}H NMR (C$_6$D$_6$, 400 MHz): δ 7.65 (br, 6H, Ar*H*), 7.42 (d, 1H, ^4J = 1.6 Hz, Ar*H*), 7.17–7.13 (m, 7H, Ar*H*, overlapped with the C$_6$D$_6$ signal), 6.99 (t, 3H, ^3J = 7.2 Hz, Ar*H*), 6.98–6.92 (m, 3H, ^3J = 7.2 Hz, Ar*H*), 6.47 (d, 1H, ^4J = 1.6 Hz, Ar*H*), 4.58 (d, 1H, ^2J = 13.8 Hz, ArC*H$_2$*N), 4.49 (d, 1H, ^2J = 12.4 Hz, NC*H$_2$*Ar), 4.10 (d, 1H, ^2J = 13.8 Hz, ArC*H$_2$*N), 3.36 (d, 1H, ^2J = 12.4 Hz, NC*H$_2$*Ar), 3.34–3.31 (m, 1H, NC*H*− of pyrrolidinyl), 2.27 (s, 6H, N(C*H$_3$*)$_2$), 2.07 (s, 3H, ArC*H$_3$*), 1.93 (m, 1H, NC*H$_2$*CH), 1.87–1.77 (m, 3H, NC*H$_2$*− of pyrrolidinyl and NC*H$_2$*CH), 1.57–1.50 (m, 1H, NCH$_2$C*H$_2$*CH$_2$CH$_3$), 1.44–1.36 (m, 1H, −C*H$_2$*− of pyrrolidinyl), 1.27–1.09 (m, 4H, NCH$_2$CH$_2$C*H$_2$*CH$_3$), 1.00 (t, 3H, NCH$_2$CH$_2$CH$_2$C*H$_3$*), 0.99–0.93 (m, 1H, −C*H$_2$*− of pyrrolidinyl), 0.90–0.82 (m, 1H, −C*H$_2$*− of pyrrolidinyl), 0.69–0.60 (m, 1H, −C*H$_2$*− of pyrrolidinyl), 0.54–0.48 (m, 1H, NCH$_2$CH$_2$C*H$_2$*CH$_3$), 0.38 (s, 18H, N[Si(C*H$_3$*)$_3$]$_2$). ^{13}C NMR (C$_6$D$_6$, 100 MHz): δ 165.0, 155.6, 135.2, 134.6, 134.5, 132.6, 132.1, 130.2, 128.2, 127.9, 127.5, 127.4, 125.0, 124.8, 121.6, 121.1, 120.2 (all Ar*C*), 64.5 (*C*Ph$_3$), 63.8 (Ar*C*H$_2$N), 59.6 (N*C*H$_2$Ar), 55.9 (N*C*H− of pyrrolidinyl), 52.5 (N*C*H$_2$− of pyrrolidinyl), 49.1 (N*C*H$_2$CH), 48.4 (N*C*H$_2$CH$_2$CH$_2$CH$_3$), 46.0 (ArN(*C*H$_3$)$_2$), 30.6 (NCH$_2$*C*H$_2$CH$_2$CH$_3$), 24.8 (−*C*H$_2$− of pyrrolidinyl), 20.9 (−*C*H$_2$− of pyrrolidinyl), 20.8 (Ar*C*H$_3$), 19.6 (NCH$_2$CH$_2$*C*H$_2$CH$_3$), 14.3 (NCH$_2$CH$_2$CH$_2$*C*H$_3$), 7.3 (N[Si(*C*H$_3$)$_3$]$_2$). Anal. Calcd for C$_{51}$H$_{70}$N$_4$OSi$_2$Zn: C, 69.87; H, 8.05; N, 6.39. Found: C, 69.76; H, 8.29; N, 6.20.

X-ray Crystallography. Single crystals of complexes **2**, **3**, **5**, and **7** were obtained from a mixture of a toluene/*n*-hexane or a benzene/*n*-hexane solution by slow evaporation at room temperature. The X-ray diffraction measurements were performed on a Bruker SMART APEX II diffractometer with graphite-monochromated Mo Kα (λ= 0.71073 Å) radiation. The data of complexes **2**, **3**, **5**. and **7** were collected at 293, 293, 140, and 173 K, respectively, using ω-scan techniques. All structures were solved by direct methods and refined using Fourier techniques. An absorption correction based on *SADABS* was applied.[27] All non-hydrogen atoms were refined by full-matrix least squares on F^2 using the *SHELXTL* program package.[28] Hydrogen atoms were located and refined by the geometry method. The cell refinement and data collection and reduction were done by Bruker *SAINT*.[29] The structure solution and refinement were performed by *SHELXS-97*[30] and *SHELXL-97*,[31] respectively. For further crystal data and details of measurements, see Table S1 in the SI. Molecular structures were generated using the *ORTEP* program.[32]

Typical Polymerization Procedure. In a glovebox, an initiator solution (0.5 mL, 10 mmol/mL) from a stock solution in toluene or THF was injected sequentially into a series of 10 mL vials loaded with *rac*-LA (0.144 g, 1.00 mmol) and a suitable amount (0.5 mL) of the same dry solvent. The mixture was stirred at room temperature and quenched at specific time intervals by adding an excess amount of normal light petroleum ether. After being dissolved with dichloromethane, a small amount of an aliquot of the bulk solution was

withdrawn and dried under reduced pressure for monomer conversion determination via ^1H NMR spectroscopy. The bulk solution was slightly concentrated and the polymer was precipitated from dichloromethane via the addition of excess methanol. The collected polymer sample was further dried in a vacuum oven at 60 °C for 16 h to a constant weight for GPC and ^1H and homonuclear-decoupled ^1H NMR analyses. In the cases where 2-propanol was used, first the monomer solution was treated with a solution of 2-propanol for 5 min, and then a solution of the initiator was injected into the mixture. Otherwise, the procedures were the same.

DOSY Experiments. DOSY experiments were carried out on a Bruker AVANCE-400 spectrometer equipped with a BBFO-*z*-atm probe having actively shielded *z*-gradient coil. Diffusion-ordered NMR data were acquired using the Bruker pulse program ledbpgp2s1d, employing a double-stimulated echo with three spoiling gradients. Sine-shaped gradient pulses were used with typical durations (P30) from 3.00 to 3.30 ms for ^1H NMR together with a diffusion period of 20 ms (D20). Gradient recovery delays of 200 μs were applied after each gradient pulse. Data were systematically accumulated by linearly varying the diffusion encoding gradients over a range from 2% to 95% for 64 gradient increment values. The signal decay dimension on the pseudo-2D data was generated by Fourier transformation of the time-domain data. DOSY plots were generated by using the DOSY processing module of TopSpin. Parameters were optimized empirically to find the best quality of data for presentation purposes. Translational diffusion coefficients (D_t) were calculated by fitting the intensity data to the Stejskal−Tanner expression.

■ ASSOCIATED CONTENT

Ⓢ Supporting Information

^1H and ^{13}C NMR spectra of all complexes and related NMR reactions, homonuclear-decoupled ^1H NMR spectra of typical polymer samples, DOSY calculation details, plots of kinetic studies of *rac*-LA polymerization by complexes **1**−**7**, and X-ray crystallographic data of complexes **2**, **3**, **5**, and **7** in CIF format. The Supporting Information is available free of charge on the ACS Publications website at DOI: 10.1021/acs.inorg-chem.5b00558. CCDC numbers 1014573 (**2**), 1014574 (**3**), 1014575 (**5**), and 1014576 (**7**) contain the supplementary crystallographic data for this paper. These data can be obtained free of charge from the Cambridge Crystallographic Data Centre via www.ccdc.cam.ac.uk/data_request/cif.

■ AUTHOR INFORMATION

Corresponding Author
*E-mail: haiyanma@ecust.edu.cn. Fax/Tel.: +86 21 64253519.

Notes
The authors declare no competing financial interest.

■ ACKNOWLEDGMENTS

■ REFERENCES

(1) (a) Ragauskas, A. J.; Williams, C. K.; Davison, B. H.; Britovsek, G.; Cairney, J.; Eckert, C. A.; Frederick, W. J.; Hallett, J. P.; Leak, D. J.; Liotta, C. L.; Mielenz, J. R.; Murphy, R.; Templer, R.; Tschaplinski, T. *Science* **2006**, *311*, 484−489. (b) Platel, R. H.; Hodgson, L. M.; Williams, C. K. *Polym. Rev.* **2008**, *48*, 11−63. (c) Ajellal, N.;

Carpentier, J.; Guillaume, C.; Guillaume, S. M.; Helou, M.; Poirier, V.; Sarazina, Y.; Trifonov, A. *Dalton Trans.* **2010**, *39*, 8363−8376. (d) Mecking, S. *Angew. Chem., Int. Ed.* **2004**, *43*, 1078−1085.

(2) (a) Inkinen, S.; Hakkarainen, M.; Albertsson, A. C.; Sodergard, A. *Biomacromolecules* **2011**, *12*, 523−532. (b) Albertsson, A. C.; Varma, I. K. *Biomacromolecules* **2003**, *4*, 1466−1486. (c) Oh, J. K. *Soft Matter* **2011**, *7*, 5096−5108. (d) Chen, F.; Hayami, J. W. S.; Amsden, B. G. *Biomacromolecules* **2014**, *15*, 1593−1601. (e) Stanford, M. J.; Dove, A. P. *Chem. Soc. Rev.* **2010**, *39*, 486−494. (f) Zhong, Z.; Dijkstra, P. J.; Feijen, J. *J. Am. Chem. Soc.* **2003**, *125*, 11291−11298.

(3) (a) Ikada, Y.; Jamshidi, K.; Tsuji, H.; Hyon, S. H. *Macromolecules* **1987**, *20*, 904−906. (b) Tsuji, H.; Horii, F.; Hyon, S. H.; Ikada, Y. *Macromolecules* **1991**, *24*, 2719−2724. (c) Fukushima, K.; Kimura, Y. *Polym. Int.* **2006**, *55*, 626−642.

(4) (a) Wachsen, O.; Reichert, K. H.; Krüger, R. P.; Muchb, H.; Schulz, G. *Polym. Degrad. Stab.* **1997**, *55*, 225−231. (b) Nomura, N.; Ishii, R.; Yamamoto, Y.; Kondo, T. *Chem.—Eur. J.* **2007**, *13*, 4433−4451.

(5) Dijkstra, P.; Du, H.; Feijen, J. *Polym. Chem.* **2011**, *2*, 520−527.

(6) Key references of isoselective catalysts for the ROP of *rac*-LA. For aluminum-based catalysts, see: (a) Spassky, N.; Wisniewski, M.; Pluta, C.; LeBorgne, A. *Macromol. Chem. Phys.* **1996**, *197*, 2627−2637. (b) Ovitt, T. M.; Coates, G. W. *J. Polym. Sci., Part A: Polym. Chem.* **2000**, *38*, 4686−4692. (c) Ovitt, T. M.; Coates, G. W. *J. Am. Chem. Soc.* **2002**, *124*, 1316−1326. (d) Zhong, Z.; Dijkstra, P. J.; Feijen, J. *Angew. Chem., Int. Ed.* **2002**, *41*, 4510−4513. (e) Zhong, Z.; Dijkstra, P. J.; Feijen, J. *J. Am. Chem. Soc.* **2003**, *125*, 11291−11298. (f) Chisholm, M. H.; Patmore, N. J.; Zhou, Z. P. *Chem. Commun.* **2005**, 127−129. (g) Chisholm, M. H.; Gallucci, J. C.; Quisenberry, K. T.; Zhou, Z. P. *Inorg. Chem.* **2008**, *47*, 2613−2624. (h) Nomura, N.; Ishii, R.; Akakura, M.; Aoi, K. *J. Am. Chem. Soc.* **2002**, *124*, 5938−5939. (i) Tang, Z.; Chen, X.; Pang, X.; Yang, Y.; Zhang, X.; Jing, X. *Biomacromolecules* **2004**, *5*, 965−970. (j) Nomura, N.; Ishii, R.; Yamamoto, Y.; Kondo, T. *Chem.—Eur. J.* **2007**, *13*, 4433−4451. (k) Pang, X.; Du, H.; Chen, X.; Wang, X.; Jing, X. *Chem.—Eur. J.* **2008**, *14*, 3126−3136. (l) Du, H. Z.; Velders, A. H.; Dijkstra, P. J.; Sun, J. R.; Zhong, Z.; Chen, X.; Feijen, J. *Chem.—Eur. J.* **2009**, *15*, 9836−9845. (m) Pilone, A.; Press, K.; Goldberg, I.; Kol, M.; Mazzeo, M.; Lamberti, M. *J. Am. Chem. Soc.* **2014**, *136*, 2940−2943. (n) Maudoux, N.; Roisnel, T.; Dorcet, V.; Carpentier, J. F.; Sarazin, Y. *Chem.—Eur. J.* **2014**, *20*, 6131−6147. For indium-based catalysts, see: (o) Douglas, A. F.; Patrick, B. O.; Mehrkhodavandi, P. *Angew. Chem., Int. Ed.* **2008**, *47*, 2290−2293. (p) Aluthge, D. C.; Patrick, B. O.; Mehrkhodavandi, P. *Chem. Commun.* **2013**, *49*, 4295−4297. (q) Yu, I.; Acosta-Ramírez, A.; Mehrkhodavandi, P. *J. Am. Chem. Soc.* **2012**, *134*, 12758−12773. For gallium-based catalysts, see: (r) Horeglad, P.; Szczepaniak, G.; Dranka, M.; Zachara, J. *Chem. Commun.* **2012**, *48*, 1171−1173.

(7) For isoselective yittrium-, zirconium-, and alkali-metal-based catalysts, see: (a) Arnold, P. L.; Buffet, J. C.; Blaudeck, R. P.; Sujecki, S.; Blake, A. J.; Wilson, C. *Angew. Chem., Int. Ed.* **2008**, *47*, 6033−6036. (b) Bakewell, C.; Cao, T.; Long, N.; Goff, X. F. L.; Auffrant, A.; Williams, C. K. *J. Am. Chem. Soc.* **2012**, *134*, 20577−20580. (c) Bakewell, C.; White, A. J.; Long, N.; Williams, C. K. *Angew. Chem., Int. Ed.* **2014**, *53*, 9226−9230. (d) Jones, M. D.; Hancock, S. L.; Mckeown, P.; Schäfer, P. M.; Buchard, A.; Thomas, L. H.; Mahon, M. F.; Lowe, J. P. *Chem. Commun.* **2014**, *50*, 15967−15970. (e) Stopper, A.; Okuda, J.; Kol, M. *Macromolecules* **2012**, *45*, 698−704. (f) Stopper, A.; Press, K.; Okuda, J.; Goldberg, I.; Kol, M. *Inorg. Chem.* **2014**, *53*, 9140−9150. (g) Zhang, J.; Xiong, J.; Sun, Y.; Tang, N.; Wu, J. *Macromolecules* **2014**, *47*, 7789−7796.

(8) For isoselective zinc-based catalysts, see: (a) Wang, H.; Ma, H. *Chem. Commun.* **2013**, *49*, 8686−8688. (b) Otero, A.; Fernandez-Baeza, J.; Sanchez-Barba, L. F.; Lara-Sanchez, A.; Tejeda, J.; Carrion, M. P.; Martinez-Ferrer, J.; Garces, A.; Rodriguez, A. M. *Organometallics* **2013**, *32*, 3437−3440. (c) Abbina, S.; Du, G. *ACS Macro Lett.* **2014**, *3*, 689−692. (d) Mou, Z.; Liu, B.; Wang, M.; Xie, H.; Li, P.; Li, S.; Cui, D. *Chem. Commun.* **2014**, *50*, 11411−11414. (e) Wang, H.; Yang, Y.; Ma, H. *Macromolecules* **2014**, *47*, 7750−7764.

(9) Key references of heteroselective catalysts for the ROP of *rac*-LA. For zinc- and magnesium-based catalysts, see: (a) Chamberlain, B. M.; Cheng, M.; Moore, D. R.; Ovitt, T. M.; Lobkovsky, E. B.; Coates, G. W. *J. Am. Chem. Soc.* **2001**, *123*, 3229–3238. (b) Chisholm, M. H.; Gallucci, J.; Phomphrai, K. *Inorg. Chem.* **2002**, *41*, 2785–2794. (c) Chen, H.-Y.; Tang, H.-Y.; Lin, C.-C. *Macromolecules* **2006**, *39*, 3745–3752. (d) Xie, H.; Mou, Z.; Liu, B.; Li, P.; Rong, W.; Li, S.; Cui, D. *Organometallics* **2014**, *33*, 722–730. For rare-earth-metal-based catalysts, see: (e) Ma, H.; Okuda, J. *Macromolecules* **2005**, *38*, 2665–2673. (f) Ma, H.; Spaniol, T. P.; Okuda, J. *Angew. Chem., Int. Ed.* **2006**, *45*, 7818–7821. (g) Ma, H.; Spaniol, T. P.; Okuda, J. *Inorg. Chem.* **2008**, *47*, 3328–3339. (h) Klitzke, J. S.; Roisnel, T.; Kirillov, E.; Casagrande, O. L., Jr.; Carpentier, J.-F. *Organometallics* **2014**, *33*, 309–321. (i) Amgoune, A.; Thomas, C. M.; Roisnel, T.; Carpentier, J. F. *Chem.—Eur. J.* **2006**, *12*, 169–179. (j) Maudoux, N.; Roisnel, T.; Carpentier, J.-F.; Sarazin, Y. *Organometallics* **2014**, *33*, 5740–5748. (k) Yang, S.; Nie, K.; Zhang, Y.; Xue, M.; Yao, Y.; Shen, Q. *Inorg. Chem.* **2014**, *53*, 105–115. (l) Liu, X.; Shang, X.; Tang, T.; Hu, N.; Pei, F.; Cui, D.; Chen, X.; Jing, X. *Organometallics* **2007**, *26*, 2747–2757. (m) Mou, Z.; Liu, B.; Liu, X.; Xie, H.; Rong, W.; Li, L.; Li, S.; Cui, D. *Macromolecules* **2014**, *47*, 2233–2241. For aluminum- and gallium-based catalysts, see: (n) Hormnirun, P.; Marshall, E. L.; Gibson, V. C.; White, A. J. P.; Williams, D. J. *J. Am. Chem. Soc.* **2004**, *126*, 2688–2689. (o) Chmura, A. J.; Chuck, C. J.; Davidson, M. G.; Jones, M. D.; Lunn, M. D.; Bull, S. D.; Mahon, M. F. *Angew. Chem., Int. Ed.* **2007**, *46*, 2280–2283.

(10) (a) Driscoll, C. T.; Schecher, W. D. *Environ. Geochem. Health* **1990**, *12*, 28–49. (b) Wu, J.; Yu, T.-L; Chen, C.-T.; Lin, C.-C. *Coord. Chem. Rev.* **2006**, *250*, 602–626.

(11) (a) Poirier, V.; Roisnel, T.; Carpentier, J.-F.; Sarazin, Y. *Dalton Trans.* **2011**, *40*, 523–534. (b) Zheng, Z.; Zhao, G.; Fablet, R.; Bouyahyi, M.; Thomas, C. T.; Roisnel, T.; Casagrande, O. J.; Carpentier, J. F. *New J. Chem.* **2008**, *32*, 2279–2291. (c) Poirier, V.; Roisnel, T.; Carpentier, J. F.; Sarazin, Y. *Dalton Trans.* **2009**, 9820–9827. (d) Wang, L.; Ma, H. *Dalton Trans.* **2010**, *39*, 7897–7910. (e) Wang, L.; Ma, H. *Macromolecules* **2010**, *43*, 6535–6537. (f) Song, S.; Zhang, X.; Ma, H.; Yang, Y. *Dalton Trans.* **2012**, *41*, 3266–3277. (g) Song, S.; Ma, H.; Yang, Y. *Dalton Trans.* **2013**, *42*, 14200–14211.

(12) For chiral zinc complexes with no isoselectivity, see: (a) Chisholm, M. H.; Eilerts, N. W.; Huffman, J. C.; Iyer, S. S.; Pacold, M.; Phomphrai, K. *J. Am. Chem. Soc.* **2000**, *122*, 11845–11854. (b) Chakraborty, D.; Chen, E. Y. X. *Organometallics* **2003**, *22*, 769–774. (c) Wu, J. C.; Huang, B. H.; Hsueh, M. L.; Lai, S. L.; Lin, C. C. *Polymer* **2005**, *46*, 9784–9792. (d) Labourdette, G.; Lee, D. J.; Patrik, B. O.; Ezhova, M. B.; Mehrkhodavandi, P. *Organometallics* **2009**, *28*, 1309–1319. (e) Darensbourg, D. J.; Karroonnirun, O. *Inorg. Chem.* **2010**, *49*, 2360–2371. (f) Drouin, F.; Oguadinma, P. O.; Whitehorne, T. J. J.; Prud'homme, R. E.; Schaper, F. *Organometallics* **2010**, *29*, 2139–2147. (g) Sun, H.; Ritch, J. S.; Hayes, P. G. *Inorg. Chem.* **2011**, *50*, 8063–8072.

(13) Cheng, M.; Attygalle, A. B.; Lobkovsky, E. B.; Coates, G. W. *J. Am. Chem. Soc.* **1999**, *121*, 11583–11584.

(14) (a) Chisholm, M. H.; Gallucci, J. C.; Phomphrai, K. *Chem. Commun.* **2003**, 48–49. (b) Chisholm, M. H.; Gallucci, J. C.; Phomphrai, K. *Inorg. Chem.* **2004**, *43*, 6717–6725.

(15) Chisholm, M. H.; Gallucci, J. C.; Zhen, H. H.; Huffman, J. C. *Inorg. Chem.* **2001**, *40*, 5051–5054.

(16) (a) Hung, W.-C.; Lin, C.-C. *Inorg. Chem.* **2009**, *48*, 728–734. (b) Tang, H.-Y.; Chen, H.-Y.; Huang, J.-H.; Lin, C.-C. *Macromolecules* **2007**, *40*, 8855–8860. (c) Yi, W.; Ma, H. *Inorg. Chem.* **2013**, *52*, 11821–11835.

(17) We chose the achiral 2-hydroxyisobutyrate instead of lactate to avoid the production of diastereomers; otherwise, the ^{1}H NMR signals will be very complicated and become inconvenient to identify the coordination pattern of the aminophenolate ligand.

(18) Chen, H.-Y.; Zhang, J.; Lin, C.-C. *Green Chem.* **2007**, *9*, 1038–1040.

(19) O'Keefe, B. J.; Brefogle, L. E.; Hillmyer, M. A.; Tolman, W. B. *J. Am. Chem. Soc.* **2002**, *124*, 4384–4393.

(20) Williams, C. K.; Brooks, N. R.; Hillmyer, M. A.; Tolman, W. B. *Chem. Commun.* **2002**, *38*, 2132–3233.

(21) Williams, C. K.; Breyfogle, L. E.; Choi, S. K.; Nam, W.; Young, V. G.; Hillmyer, M. A.; Tolman, W. B. *J. Am. Chem. Soc.* **2003**, *125*, 11350–11359.

(22) (a) Pilone, A.; Lamberti, M.; Mazzeo, M.; Milione, S.; Pellecchia, C. *Dalton Trans.* **2013**, *42*, 13036–13047. (b) Roşca, S.-C.; Roşca, D.-A.; Dorcet, V.; Kozak, C. M.; Kerton, F. M.; Carpentier, J.-F.; Sarazin, Y. *Dalton Trans.* **2013**, *42*, 9361–9375.

(23) (a) This reference allows one to take into account the variation in the solvent properties with changing solute concentrations or mixture composition, making it possible to correct the measured diffusion values for any changes in the viscosity. (b) Macchioni, A.; Ciancaleoni, G.; Zuccaccia, C.; Zuccaccia, D. *Chem. Soc. Rev.* **2008**, *37*, 479–489.

(24) The resonance of the C=O moiety in the ^{13}C{^{1}H} NMR spectrum of the in situ generated (L^7)Zn(OCMe$_2$COOMe) in C$_6$D$_6$ was not observed, possibly because of a low resolution.[9a]

(25) (a) Dove, A. P.; Gibson, V. C.; Marshall, E. L.; Rzepa, H. S.; White, A. J. P.; Williams, D. J. *J. Am. Chem. Soc.* **2006**, *128*, 9834–9843. (b) Wang, L.; Kefalidis, C. E.; Sinbandhit, S.; Dorcet, V.; Carpentier, J.-F.; Maron, L.; Sarazin, Y. *Chem.—Eur. J.* **2013**, *19*, 13463–13478.

(26) We found it was not suitable to use Mark−Houwink corrections in these cases because the measured molecular weights of PLAs obtained by other initiators, such as aluminum initiators, were well-matched to the theoretical values.

(27) *SADABS, Bruker Nonius area detector scaling and absorption correction*, version 2.05; Bruker AXS Inc.: Madison, WI, 1996.

(28) Sheldrick, G. M. *SHELXTL 5.10 for Windows NT, Structure Determination Software Programs*; Bruker Analytical X-ray Systems, Inc.: Madison, WI, 1997.

(29) *SAINT*, version 6.02; Bruker AXS Inc.: Madison, WI, 1999.

(30) Sheldrick, G. M. *SHELXS-97, Program for the Solution of Crystal Structures*; University of Göttingen: Göttingen, Germany, 1990.

(31) Sheldrick, G. M. *SHELXL-97, Program for the Refinement of Crystal Structures*; University of Göttingen: Göttingen, Germany, 1997.

(32) Farrugia, L. J. *J. Appl. Crystallogr.* **1997**, *30*, 565. *ORTEP-III for Windows*, version 2.0; University of Glasgow: Glasgow, Scotland, 2008.